

Channel Estimation and Data Decoding Analysis of Massive MIMO with 1-Bit ADCs

Italo Atzeni, *Member, IEEE* and Antti Tölli, *Senior Member, IEEE*

Abstract

We present an analytical framework for the channel estimation and the data decoding in massive multiple-input multiple-output uplink systems with 1-bit analog-to-digital converters (ADCs). First, we provide a closed-form expression of the mean squared error of the channel estimation for a general class of linear estimators. In addition, we propose a novel linear estimator with significantly enhanced performance compared with existing estimators with the same structure. For the data decoding, we provide closed-form expressions of the expected value and the variance of the estimated symbols when maximum ratio combining is adopted, which can be exploited to efficiently implement maximum likelihood decoding and, potentially, to design the set of transmit symbols. Comprehensive numerical results are presented to study the performance of the channel estimation and the data decoding with 1-bit ADCs with respect to the signal-to-noise ratio (SNR), the number of user equipments, and the pilot length. The proposed analysis highlights a fundamental SNR trade-off, according to which operating at the right noise level significantly enhances the system performance.

I. INTRODUCTION

The migration of operating frequencies from first- to fourth-generation wireless systems, i.e., from 800 MHz to the sub-3 GHz range, did not bring major changes in terms of signal propagation. The current fifth generation (5G) features a more pronounced transition in this respect by operating at sub-6 GHz frequencies and, eventually, up to 30 GHz with the objective of boosting the data rates. Following this trend, beyond-5G systems will exploit the large amount of bandwidth available in the mmWave band (i.e., 30 GHz–300 GHz) and raise the operating frequencies up to 1 THz [1]. However, as the free-space pathloss scales as the square of the frequency, maintaining the same signal-to-noise ratio (SNR) over a given distance will require increasingly sharp beamforming to spatially focus the signal power. Although the short wavelength at mmWave and THz frequencies allows to pack many antennas into a very small area, realizing fully digital, high-resolution massive multiple-input multiple-output (MIMO) arrays remains prohibitive in practice [2], [3].

The authors are with the Centre for Wireless Communications, University of Oulu, Finland (emails: {italo.atzeni, antti.tolli}@oulu.fi). The work of I. Atzeni was supported by the Marie Skłodowska-Curie Actions (MSCA-IF 897938 DELIGHT). The work of A. Tölli was supported by the Academy of Finland under grant no. 318927 (6Genesis Flagship).

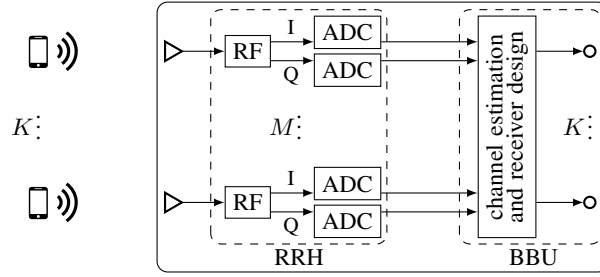


Fig. 1: Massive MIMO uplink system model with 1-bit ADCs.

As in the system model illustrated in Fig. 1, each base station (BS) antenna is generally equipped with a dedicated radio-frequency (RF) chain that includes complex, power-hungry analog-to-digital/digital-to-analog converters (ADCs/DACs) [3]. In this setting, while the transmit power can be made inversely proportional to the number of antennas, the power dissipated by each ADC/DAC scales linearly with the sampling rate and exponentially with the number of quantization bits [4]–[8]. Another limiting factor is the amount of raw data exchanged between the remote radio head (RRH) and the base-band unit (BBU), which scales linearly with both the sampling rate and the number of quantization bits [9]–[11]. For these reasons, adopting low-resolution ADCs/DACs with 1 to 4 quantization bits as opposed to the typical 10 or more [12] enables the implementation of massive MIMO arrays comprising hundreds (or even thousands) of antennas, which are necessary to operate in the mmWave and THz bands [9]. In this regard, 1-bit ADCs/DACs are particularly appealing due to their minimal power consumption and complexity since they only evaluate the sign of the input signal [4]. Such a coarse quantization is especially motivated at very high frequencies, where high-order modulations are not essential.

There is a large body of literature on massive MIMO with low-resolution and 1-bit ADCs/DACs, ranging from performance analysis to channel estimation and precoding design. The capacity of the 1-bit quantized MIMO channel is characterized in [4], whereas [13] shows that replacing even a small number of high-resolution ADCs with 1-bit ADCs entails a modest performance loss while significantly reducing the power consumption. [5] studies the performance-quantization trade-off of orthogonal frequency-division multiplexing (OFDM) uplink systems and shows that using 4 to 6 quantization bits involves almost no performance loss compared with infinite-resolution ADCs. The spectral efficiency of single-carrier and OFDM uplink systems with 1-bit ADCs is analyzed in [14]. The problem of multi-user detection is considered, e.g., in [15] and [16] for low-resolution and 1-bit ADCs, respectively, whereas [17] focuses on the joint channel estimation and data decoding. [6] proposes an efficient iterative method for near maximum likelihood decoding (MLD)

with 1-bit ADCs. The work in [7] analyzes the channel estimation and the uplink achievable rate with 1-bit ADCs. In addition, it proposes a linear channel estimator based on the Bussgang decomposition, which allows to reformulate the nonlinear quantization function as a linear function with identical first- and second-order statistics [18]. A similar analysis is presented in [19] for the downlink direction. [9] extends some of the results derived in [7], [14] for 1-bit ADCs to the multi-bit case. Specifically, it presents a throughput analysis of uplink systems and proposes a linear channel estimator based on the Bussgang decomposition with low-resolution ADCs. The channel estimation with 1-bit ADCs when the quantization threshold is not known is studied in [20]. The channel estimation exploiting the angular and delay structure is considered in [21] and [22] for low-resolution and 1-bit ADCs, respectively. A recent line of works employs machine learning techniques in scenarios where obtaining accurate channel state information with low-resolution ADCs is impractical (see, e.g., [23], [24]). [8] analyzes the performance of linear precoding schemes for downlink systems with 1-bit DACs. A similar analysis with multi-bit DACs is presented in [10] considering both linear and nonlinear precoding, and in [11] considering linear precoding with oversampling in OFDM downlink systems. Lastly, [25] proposes a general optimization framework for downlink precoding with 1-bit DACs and constant envelope assuming quadrature amplitude modulation (QAM) transmit symbols.

A. Contribution

This paper broadens prior analytical studies on the channel estimation and the data decoding in massive MIMO uplink systems with 1-bit ADCs. On the one hand, existing works do not provide exact expressions of the mean squared error (MSE) of the channel estimation, which makes it difficult to analyze its performance with respect to different parameters. We fill this gap by deriving such an expression for a general class of linear estimators with the structure of the one proposed in [14], which can be obtained from the state-of-the-art linear estimator in [7] by ignoring the temporal correlation of the quantization distortion. As a valuable side product, we obtain a new estimator with the same simple structure but with significantly better accuracy. On the other hand, in the context of data decoding, existing works fail to characterize the statistical properties of the estimated symbols. In this regard, an interesting SNR trade-off was observed in [9], whereby the estimated symbols resulting from transmit symbols with the same phase overlap at high SNR; however, this aspect has not been formally described in the literature. We fill this gap by analyzing the expected value and the variance of the estimated symbols along with their asymptotic behavior

at high SNR. These results ultimately impact the symbol error rate (SER) and thus provide important practical insights into the design and the implementation of 1-bit quantized systems.

The contributions of this paper are summarized as follows:

- For the channel estimation with 1-bit ADCs, we derive a general closed-form expression of the MSE for linear estimators with the structure of the one proposed in [14]. This enables a precise characterization of the performance of the channel estimation with respect to the SNR, the number of user equipments (UEs), and the pilot length.
- Using the above result, we propose a novel linear estimator with the same simple structure of the one proposed in [14] but significantly enhanced performance in terms of MSE. Through numerical simulations with uncorrelated channels, we show that our proposed estimator achieves the same accuracy as the (more complex) estimator proposed in [7].
- For the data decoding with 1-bit ADCs, we characterize the statistical properties of the estimated symbols by deriving closed-form expressions of the expected value and the variance when maximum ratio combining (MRC) is adopted at the BS. These can be exploited to efficiently implement MLD and, potentially, to design the set of transmit symbols.
- Building on the proposed analysis, we provide a thorough discussion on the effect of 1-bit quantization on both the channel estimation and the data decoding. For each of the two aspects, we describe a fundamental SNR trade-off, according to which operating at the right noise level significantly enhances the system performance. In this respect, the optimal transmit SNR for the channel estimation is shown to decrease as the pilot length increases.

Outline. The rest of the paper is structured as follows. Section II introduces the system model with 1-bit ADCs. Sections III and IV present our performance analysis results on the channel estimation and the data decoding, respectively, each including dedicated numerical results and discussion. Finally, Section V summarizes our contributions and draws some concluding remarks.

Notation. $\mathbf{A} = (A_{m,n})$ specifies that $A_{m,n}$ is the (m,n) th entry of matrix \mathbf{A} ; likewise, $\mathbf{a} = (a_n)$ specifies that a_n is the n th entry of vector \mathbf{a} . $(\cdot)^T$, $(\cdot)^H$, and $(\cdot)^*$ represent the transpose, Hermitian transpose, and conjugate operators, respectively. $\text{Re}[\cdot]$ and $\text{Im}[\cdot]$ denote the real part and imaginary part operators, respectively, whereas j is the imaginary unit. $\mathbb{E}[\cdot]$ and $\mathbb{V}[\cdot]$ are the expectation and variance operators, respectively. \mathbf{I}_N , $\mathbf{0}_N$, and $\mathbf{1}_N$ denote the N -dimensional identity matrix, all-zero vector, and all-one vector, respectively. $\text{sgn}(\cdot)$ is the sign function and $(a \bmod b)$ denotes the modulo operator, whereas $\{\cdot\}$ is used to represent sets. $\text{vec}[\cdot]$ is the vectorization operator,

whereas \otimes denotes the Kronecker product. Lastly, $\mathcal{N}(\mathbf{0}_N, \Sigma)$ and $\mathcal{CN}(\mathbf{0}_N, \Sigma)$ are the real and complex N -variate normal distributions with zero mean and covariance matrix Σ , respectively.

II. SYSTEM MODEL

Consider the scenario depicted in Fig. 1, where a BS with M antennas serves K single-antenna UEs in the uplink. Let $\mathbf{H} \triangleq (H_{m,k}) \in \mathbb{C}^{M \times K}$ denote the uplink channel matrix whose entries are assumed to be distributed independently as $\mathcal{CN}(0, 1)$ (as, e.g., in [7], [9]–[11]). Each UE transmits with power ρ and the additive white Gaussian noise (AWGN) at the BS has unit variance: thus, ρ can be interpreted as the transmit SNR. Note that the same transmit SNR is assumed for the two phases of channel estimation and uplink data transmission. Each BS antenna is connected with two 1-bit ADCs, one for the in-phase component and one for the quadrature component of the receive signal. Therefore, according to [9], we introduce the 1-bit quantization function $Q(\cdot) : \mathbb{C}^{L \times N} \rightarrow \mathcal{Q}$, with

$$Q(\mathbf{A}) \triangleq \sqrt{\frac{\rho K + 1}{2}} \left(\text{sgn}(\text{Re}[\mathbf{A}]) + j \text{sgn}(\text{Im}[\mathbf{A}]) \right) \quad (1)$$

and where $\mathcal{Q} \triangleq \sqrt{\frac{\rho K + 1}{2}} \{\pm 1 \pm j\}^{L \times N}$ is the set containing the scaled symbols of the quadrature phase-shift keying (QPSK) constellation.

A. Channel Estimation

In the channel estimation phase, the UEs simultaneously transmit their uplink pilots of length τ . Let $\mathbf{P} \triangleq (P_{u,k}) \in \mathbb{C}^{\tau \times K}$ denote the pilot matrix whose columns correspond to the pilots used by the UEs, with $|P_{u,k}|^2 = 1, \forall u, k$: assuming $\tau \geq K$ and orthogonal pilots among the UEs, we have $\mathbf{P}^H \mathbf{P} = \tau \mathbf{I}_K$. Hence, the receive signal at the BS prior to quantization is given by

$$\mathbf{Y}_p \triangleq \sqrt{\rho} \mathbf{H} \mathbf{P}^H + \mathbf{Z}_p \in \mathbb{C}^{M \times \tau} \quad (2)$$

where $\mathbf{Z}_p \triangleq (Z_{m,u}) \in \mathbb{C}^{M \times \tau}$ is the AWGN matrix with entries distributed as $\mathcal{CN}(0, 1)$. Then, at the output of the ADCs, we have

$$\mathbf{R}_p \triangleq Q(\mathbf{Y}_p) \in \mathbb{C}^{M \times \tau} \quad (3)$$

with $\mathbf{R}_p = (R_{m,u})$, which is used by the BS to estimate \mathbf{H} . Some comments are in order. Firstly, correlating the quantized receive signal \mathbf{R}_p in (3) with \mathbf{P} (as done next in (5) and (17)) results in residual pilot contamination even when the pilots are orthogonal (see, e.g., [14]). Secondly, the pilots should be preferably chosen such that their entries span the unit circle so as to accurately estimate the phases, especially at high SNR. This is explained in Appendix I, which provides a detailed discussion on the channel estimation with 1-bit ADCs.

A linear minimum MSE (MMSE) estimator based on the Bussgang decomposition (see [18]), which we refer to as Bussgang linear MMSE (BLM) estimator, was proposed in [7], whereby $\underline{\mathbf{h}} \triangleq \text{vec}[\mathbf{H}] \in \mathbb{C}^{MK \times 1}$ is estimated as

$$\hat{\underline{\mathbf{h}}}^{\text{BLM}} \triangleq \sqrt{\frac{2}{\pi}} \rho \bar{\mathbf{P}}^T \Sigma_{\mathbf{p}}^{-1} \underline{\mathbf{r}}_{\mathbf{p}} \in \mathbb{C}^{MK \times 1} \quad (4)$$

with $\bar{\mathbf{P}} \triangleq \mathbf{P} \otimes \mathbf{I}_M \in \mathbb{C}^{M\tau \times MK}$ and $\underline{\mathbf{r}}_{\mathbf{p}} \triangleq \text{vec}[\mathbf{R}_{\mathbf{p}}] \in \mathbb{C}^{M\tau \times 1}$, and where $\Sigma_{\mathbf{p}} \triangleq \mathbb{E}[\underline{\mathbf{r}}_{\mathbf{p}} \underline{\mathbf{r}}_{\mathbf{p}}^H] \in \mathbb{C}^{M\tau \times M\tau}$ denotes the covariance matrix of $\underline{\mathbf{r}}_{\mathbf{p}}$.¹ A linear estimator with a simpler structure can be obtained from (4) by ignoring the temporal correlation of the quantization distortion, which implies that the off-diagonal entries of $\Sigma_{\mathbf{p}}$ are zero. Such an estimator was proposed in [14] (and later extended to the case of multi-bit ADCs in [9]), whereby \mathbf{H} is estimated as

$$\hat{\mathbf{H}} \triangleq \sqrt{\Psi} \mathbf{R}_{\mathbf{p}} \mathbf{P} \in \mathbb{C}^{M \times K} \quad (5)$$

where we have defined

$$\Psi \triangleq \frac{2}{\pi} \rho \left(\frac{2}{\pi} \rho (\tau - K) + \rho K + 1 \right)^{-2}. \quad (6)$$

Note that, when $\tau = K$, (5) coincides with (4) since $\Sigma_{\mathbf{p}} = (\rho K + 1) \mathbf{I}_{MK}$; otherwise, (5) accurately approximates (4) at low SNR or when K is large [9]. Due to the presence of $\Sigma_{\mathbf{p}}^{-1}$, it is difficult to analyze the performance of the BLM estimator in (4) with respect to the different parameters. Hence, in Section III, we focus on analyzing the estimator in (5); in addition, we propose a new estimator that is characterized by the same simple structure but with significantly better accuracy.

B. Uplink Data Transmission

Let $x_k \in \mathbb{C}$ be the transmit symbol of UE k , with $\mathbb{E}[|x_k|^2] = 1$ and $\mathbf{x} \triangleq (x_k) \in \mathbb{C}^{K \times 1}$. The receive signal at the BS prior to quantization is given by

$$\mathbf{y} \triangleq \sqrt{\rho} \mathbf{H} \mathbf{x} + \mathbf{z} \in \mathbb{C}^{M \times 1} \quad (7)$$

where $\mathbf{z} \triangleq (z_m) \in \mathbb{C}^{M \times 1}$ is the AWGN term with entries distributed as $\mathcal{CN}(0, 1)$. Then, at the output of the ADCs, we have

$$\mathbf{r} \triangleq Q(\mathbf{y}) \in \mathbb{C}^{M \times 1} \quad (8)$$

and the BS obtains a soft estimate of \mathbf{x} as

$$\hat{\mathbf{x}} \triangleq \mathbf{V}^H \mathbf{r} \in \mathbb{C}^{K \times 1} \quad (9)$$

where $\mathbf{V} \in \mathbb{C}^{M \times K}$ is the combining matrix adopted at the BS. Finally, the decoding process associates each estimated symbol to a transmit symbol (e.g., via MLD). In Section IV, we focus on

¹Note that, in case of correlated channels, the channel covariance can be embedded into (4) as described in [7].

characterizing the statistical properties of the estimated symbols when MRC is adopted at the BS.

III. CHANNEL ESTIMATION WITH 1-BIT ADCs

In this section, we are interested in characterizing the performance of the channel estimation with respect to the different parameters when 1-bit ADCs are adopted at each BS antenna (see Section II-A). In this regard, we focus on the estimator in (5) since the presence of Σ_p^{-1} considerably complicates the analysis of the BLM estimator in (4). Subsequently, we propose a novel estimator with the same simple structure of (5) and significantly improved accuracy. To this end, we first introduce the following proposition, which will be used to prove several of our results in this section and in Section IV.

Proposition 1. Let $\zeta \sim \mathcal{N}(0, \alpha \mathbf{I}_N)$ with $\alpha > 0$. For $\mathbf{a}_1, \mathbf{a}_2 \in \mathbb{R}^{N \times 1}$, we have

$$\mathbb{E}[\text{sgn}(\mathbf{a}_1^T \zeta) \text{sgn}(\mathbf{a}_2^T \zeta)] = \Omega \left(\frac{\mathbf{a}_1^T \mathbf{a}_2}{\|\mathbf{a}_1\| \|\mathbf{a}_2\|} \right) \quad (10)$$

where we have defined

$$\Omega(w) \triangleq \frac{2}{\pi} \arcsin(w). \quad (11)$$

Proof: See Appendix II. ■

A. MSE of the Channel Estimation

The (normalized) MSE of the channel estimation when (5) is used is defined as

$$\text{MSE}_p \triangleq \frac{1}{MK} \mathbb{E}[\|\hat{\mathbf{H}} - \mathbf{H}\|_F^2]. \quad (12)$$

In [9, Eq. (23)] and in [7, Eq. (17)], the closed-form expression of (12) was derived for the case of $\tau = K$, which gives

$$\text{MSE}_p = 1 - \frac{2}{\pi} \frac{\rho K}{\rho K + 1}. \quad (13)$$

Note that the above expression is lower bounded by $1 - \frac{2}{\pi} \simeq 0.363$, which is achieved in the limit of $\rho K \rightarrow \infty$. Hence, in realistic scenarios (especially for small values of K), using a pilot length that is equal to the number of UEs results in quite inaccurate channel estimates. In general, τ should be sufficiently large to compensate for the low granularity of the ADCs, as detailed in Appendix I. For this reason, we derive a general closed-form expression of (12) when an estimator with the structure of (5) is used, which is valid for any value of τ and K .

Theorem 1. Suppose that the estimator in (5) is used with arbitrary Ψ . Then, the MSE of the channel estimation in (12) is given by

$$\text{MSE}_p = 1 + (\rho K + 1)\Psi(\tau + \Delta) - 2\sqrt{\frac{2}{\pi}}\rho\Psi\tau \quad (14)$$

where we have defined

$$\Delta \triangleq \frac{1}{K} \sum_{k=1}^K \sum_{u \neq v} \left(\text{Re}[P_{u,k}^* P_{v,k}] \Omega \left(\frac{\rho \sum_{i=1}^K \text{Re}[P_{u,i} P_{v,i}^*]}{\rho K + 1} \right) - \text{Im}[P_{u,k}^* P_{v,k}] \Omega \left(\frac{\rho \sum_{i=1}^K \text{Im}[P_{u,i} P_{v,i}^*]}{\rho K + 1} \right) \right). \quad (15)$$

Proof: See Appendix III. ■

The result of Theorem 1 enables a precise characterization of the performance of estimators with the structure of (5), i.e., with arbitrary Ψ , with respect to the transmit SNR ρ , the number of UEs K , and the pilot length τ . In particular, when Ψ defined in (6) is used, (14) becomes

$$\text{MSE}_p = 1 - \frac{2}{\pi} \rho \left(\frac{2}{\pi} \rho (\tau - K) + \rho K + 1 \right)^{-2} \left(\frac{4}{\pi} \rho \tau (\tau - K) + (\rho K + 1)(\tau - \Delta) \right). \quad (16)$$

When $\tau = K$, (16) recovers the expression in (13): in fact, $\tau = K$ implies $\Delta = 0$ since $\sum_{i=1}^K P_{u,i} P_{v,i}^* = 0$, $\forall u \neq v$. Moreover, we point out that the parameter Δ in (15) is roughly proportional to $\tau(\tau - 1)$.

Now, if we consider Ψ as a tuning parameter, we can minimize MSE_p in (14) by optimizing over Ψ . As a result, we obtain a novel estimator that is characterized by the same simple structure of (5) and enhanced performance in terms of MSE.

Theorem 2. Suppose that the estimator

$$\hat{\mathbf{H}}' \triangleq \sqrt{\Psi'} \mathbf{R}_p \mathbf{P} \in \mathbb{C}^{M \times K} \quad (17)$$

is used, where Ψ' is obtained by minimizing (14) with respect to Ψ and is defined as

$$\Psi' \triangleq \frac{2}{\pi} \frac{\rho}{(\rho K + 1)^2} \frac{\tau^2}{(\tau + \Delta)^2} \quad (18)$$

with Δ defined in (15). Then, the MSE of the channel estimation is given by

$$\text{MSE}_p' \triangleq \frac{1}{MK} \mathbb{E}[\|\hat{\mathbf{H}}' - \mathbf{H}\|_F^2] \quad (19)$$

$$= 1 - \frac{2}{\pi} \frac{\rho \tau^2}{(\rho K + 1)(\tau + \Delta)} \quad (20)$$

$$\leq \text{MSE}_p \quad (21)$$

with MSE_p given in (16).

Proof: Since (14) is a convex function of Ψ , Ψ' in (18) can be obtained by setting $\frac{d}{d\Psi} \text{MSE}_p = 0$. Then, since (16) is a special case of (14), it follows that $\text{MSE}_p' \leq \text{MSE}_p$. ■

When $\tau = K$, our proposed estimator in (17) coincides with the estimator in (5), and, in turn,

with the BLM estimator in (4): in fact, $\tau = K$ implies that Ψ' in (18) reduces to Ψ in (6) and (20) recovers the expression in (13). Since Ψ' results from the optimization of (14) over Ψ , our proposed estimator shall be always preferred to the estimator in (5), and the performance gap between the two widens with $\tau - K$. Furthermore, the associated MSE expression in (20) turns out to be more tractable than its counterpart in (16). Remarkably, in Section III-C, we show numerically that our proposed estimator achieves the same accuracy as the BLM estimator in (4).

It is of particular interest to study the asymptotic behavior of the MSE of the channel estimation at high SNR.

Corollary 1. From Theorems 1 and 2, in the limit of $\rho \rightarrow \infty$, we have

$$\lim_{\rho \rightarrow \infty} \text{MSE}_p = 1 - \frac{2}{\pi} \left(\frac{2}{\pi} (\tau - K) + K \right)^{-2} \left(\frac{4}{\pi} \tau (\tau - K) + K(\tau - \bar{\Delta}) \right) \quad (22)$$

and

$$\lim_{\rho \rightarrow \infty} \text{MSE}'_p = 1 - \frac{2}{\pi} \frac{\tau^2}{K(\tau + \bar{\Delta})} \quad (23)$$

where we have defined

$$\bar{\Delta} \triangleq \frac{1}{K} \sum_{k=1}^K \sum_{u \neq v} \left(\text{Re}[P_{u,k}^* P_{v,k}] \Omega \left(\frac{\sum_{i=1}^K \text{Re}[P_{u,i} P_{v,i}^*]}{K} \right) - \text{Im}[P_{u,k}^* P_{v,k}] \Omega \left(\frac{\sum_{i=1}^K \text{Im}[P_{u,i} P_{v,i}^*]}{K} \right) \right). \quad (24)$$

The results of Corollary 1 show that arbitrarily increasing the transmit SNR is detrimental for the performance of the channel estimation, since the right amount of noise is necessary to recover the difference in amplitude between channel entries (see Appendix I). This is in sheer contrast with the case of infinite-resolution ADCs, where boosting ρ produces the same beneficial noise-averaging effect as increasing τ .

B. Tractable Upper Bounds

The MSE expressions derived so far depend on the specific pilot choice through the parameter Δ in (15). To gain more practical insights, we now consider the single-UE case (i.e., $K = 1$) where $\mathbf{p} \triangleq (p_u) \in \mathbb{C}^{\tau \times 1}$ denotes the pilot used by the UE. In this setting, tractable upper bounds on the MSE expressions can be obtained by fixing \mathbf{p} such that $p_u \in \{\pm\beta, \pm j\beta\}$, $\forall u$, where $\beta \in \mathbb{C}$ and $|\beta|^2 = 1$; in the rest of the paper, when referring to this case, we will simply use $\mathbf{p} = \mathbf{1}_\tau$. In fact, as detailed in Appendix I, such a structure of \mathbf{p} represents the worst possible pilot choice, especially at high SNR. Hence, from (15), we have

$$\Delta = \tau(\tau - 1) \Omega \left(\frac{\rho}{\rho + 1} \right) \quad (25)$$

and, plugging (25) into (16) and (22) yields

$$\text{MSE}_p = 1 - \frac{2}{\pi} \rho \tau \left(\frac{2}{\pi} \rho (\tau - 1) + \rho + 1 \right)^{-2} \left(\frac{4}{\pi} \rho (\tau - 1) + (\rho + 1) \left(1 - (\tau - 1) \Omega \left(\frac{\rho}{\rho + 1} \right) \right) \right) \quad (26)$$

and

$$\lim_{\rho \rightarrow \infty} \text{MSE}_p = 1 - \frac{2}{\pi} \tau \left(\frac{2}{\pi} (\tau - 1) + 1 \right)^{-2} \left(\frac{4}{\pi} (\tau - 1) - \tau + 2 \right) \quad (27)$$

respectively. In addition, considering (26) in the limit of $\tau \rightarrow \infty$, we have

$$\lim_{\tau \rightarrow \infty} \text{MSE}_p = \frac{\pi}{2} \frac{\rho + 1}{\rho} \Omega \left(\frac{\rho}{\rho + 1} \right) - 1. \quad (28)$$

Likewise, plugging (25) into (20) and (23) yields

$$\text{MSE}'_p = 1 - \frac{2}{\pi} \frac{\rho \tau}{(\rho + 1) \left(1 + (\tau - 1) \Omega \left(\frac{\rho}{\rho + 1} \right) \right)} \quad (29)$$

and

$$\lim_{\rho \rightarrow \infty} \text{MSE}'_p = 1 - \frac{2}{\pi} \quad (30)$$

respectively. In addition, considering (29) in the limit of $\tau \rightarrow \infty$, we have

$$\lim_{\tau \rightarrow \infty} \text{MSE}'_p = 1 - \frac{2}{\pi} \frac{\rho}{(\rho + 1) \Omega \left(\frac{\rho}{\rho + 1} \right)}. \quad (31)$$

Some comments are in order. Firstly, when $\tau = 1$, both (26) and (29) recover the expression in (13) with $K = 1$. Secondly, (30) does not depend on τ since, in the absence of noise, estimating the channel repeatedly over the same pilot symbol does not bring any benefit. Thirdly, it can be shown that (26) and (29) are quasiconvex functions of ρ and, as such, they have a unique minimum. This defines a clear SNR trade-off, according to which operating at the right noise level enhances the channel estimation accuracy. In particular, as discussed in Appendix I, we have that:

- At low SNR, the channel estimates are corrupted by the strong noise;
- At high SNR, the difference in amplitude between channel entries cannot be recovered.

In general, for $\tau > 1$, the value of ρ that minimizes (29), denoted by ρ^* , satisfies

$$\frac{2}{\pi} \frac{\rho^*}{\sqrt{1 + 2\rho^*}} - \Omega \left(\frac{\rho^*}{\rho^* + 1} \right) = \frac{1}{\tau - 1}. \quad (32)$$

Since the left-hand side of (32) monotonically increases with the transmit SNR, ρ^* decreases as the left-hand side of (32) decreases, i.e., as τ increases. This means that using longer pilots allows to operate at lower SNR as the noise can be averaged out more efficiently. This interdependence between ρ and τ can be also observed from (31): in the limit of $\tau \rightarrow \infty$, since $\lim_{w \rightarrow 0} \frac{w}{\arcsin(w)} = 1$, it follows that $\text{MSE}'_p \rightarrow 0$ as $\rho \rightarrow 0$. Lastly, it is shown in Section III-C that the upper bounds obtained by fixing $\mathbf{p} = \mathbf{1}_\tau$ are remarkably tight at low SNR and up to the region around the

optimal value of ρ . Therefore, the above observations also apply to the general case.

C. Numerical Results and Discussion

We now focus on the performance evaluation of the channel estimation with 1-bit ADCs with respect to the different parameters based on the analytical results presented in Sections III-A and III-B. In this regard, when $K > 1$, we use a pilot matrix \mathbf{P} composed of the first K columns of the τ -dimensional discrete Fourier transform (DFT) matrix; however, we remark that our analytical framework is valid for any choice of \mathbf{P} satisfying $\mathbf{P}^H \mathbf{P} = \tau \mathbf{I}_K$ and $|P_{u,k}|^2 = 1, \forall u, k$.² On the other hand, when $K = 1$, we use the pilots $\mathbf{p} = \mathbf{d}_2$, where

$$\mathbf{d}_2 \triangleq [1, e^{-j \frac{2\pi}{\tau}}, e^{-j 2 \frac{2\pi}{\tau}}, \dots, e^{-j (\tau-1) \frac{2\pi}{\tau}}]^T \in \mathbb{C}^{\tau \times 1} \quad (33)$$

denotes the second column of the τ -dimensional DFT matrix, and $\mathbf{p} = \mathbf{1}_\tau$: these represent the best and the worst possible pilot choices, respectively (see Appendix I for more details on the pilot choice). We thus consider the expressions of $\text{MSE}_{\mathbf{p}}$ derived in (16), resulting from the estimator in (5) (see [14]), and $\text{MSE}'_{\mathbf{p}}$ derived in (20), resulting from our proposed estimator in (17). In addition, we consider the MSE of the channel estimation resulting from the BLM estimator in (4) (see [7]), defined as

$$\text{MSE}_{\mathbf{p}}^{\text{BLM}} \triangleq \frac{1}{MK} \|\hat{\mathbf{h}}^{\text{BLM}} - \mathbf{h}\|^2 \quad (34)$$

which we compute numerically by means of Monte Carlo simulations with 10^6 independent channel realizations. To facilitate the computation of the channel estimates as in (4), we derive the closed-form expression of $\Sigma_{\mathbf{p}}$ in the following proposition.

Proposition 2. Suppose that the entries of \mathbf{H} are distributed independently as $\mathcal{CN}(0, 1)$. Then, the covariance matrix of $\mathbf{r}_{\mathbf{p}}$ can be written as

$$\Sigma_{\mathbf{p}} = (\rho K + 1) \Phi \otimes \mathbf{I}_M \quad (35)$$

where we have defined $\Phi \triangleq (\Phi_{u,v}) \in \mathbb{C}^{\tau \times \tau}$, with

$$\Phi_{u,v} \triangleq \Omega \left(\frac{\rho \sum_{k=1}^K \text{Re}[P_{u,k} P_{v,k}^*]}{\rho K + 1} \right) - j \Omega \left(\frac{\rho \sum_{k=1}^K \text{Im}[P_{u,k} P_{v,k}^*]}{\rho K + 1} \right). \quad (36)$$

Proof: See Appendix IV. ■

The result of Proposition 2 allows to avoid the numerical computation of $\Sigma_{\mathbf{p}}$, which significantly simplifies the computation of the channel estimates with the BLM estimator.³ Nonetheless, the

²For instance, one can use orthogonal Zadoff-Chu sequences, which are widely adopted in the LTE air interface [26].

³Note that, according to Proposition 2 and the properties of the Kronecker product, we can write $\Sigma_{\mathbf{p}}^{-1} = \frac{1}{\rho K + 1} \Phi^{-1} \otimes \mathbf{I}_M$.

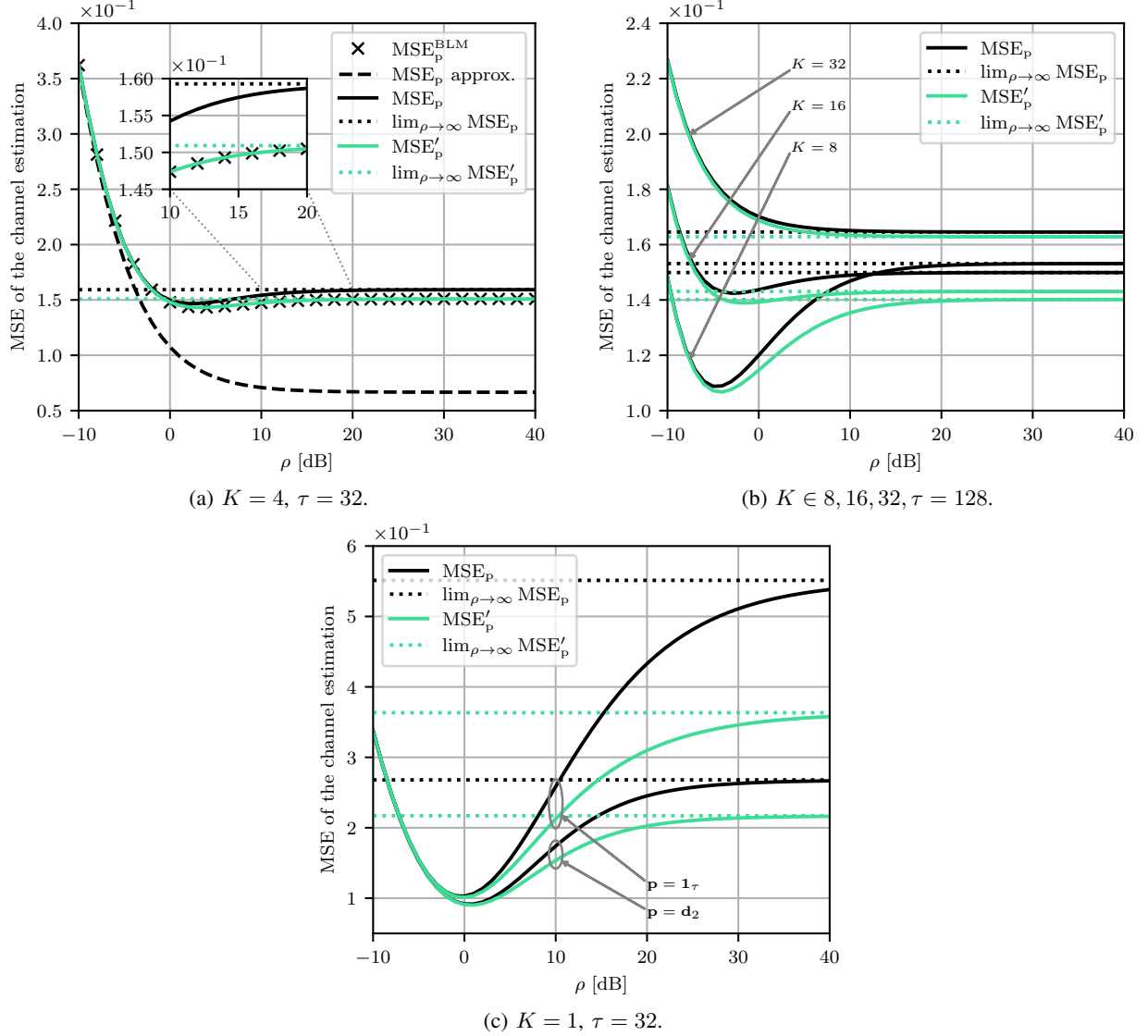


Fig. 2: MSE of the channel estimation against the transmit SNR.

complexity involved in obtaining $\text{MSE}_p^{\text{BLM}}$ in (34) via Monte Carlo simulations with reasonable accuracy remains prohibitive for large values of K and τ . Fig. 2 illustrates the MSE of the channel estimation against the transmit SNR ρ , also including the asymptotic MSE expressions in (22) and (23). Fig. 2(a) considers $K = 4$ and $\tau = 32$; here “ MSE_p approx.” indicates the approximated MSE expression in [9, Eq. (23)], which is exact when $\tau = K$. We begin by observing that our proposed estimator in (17) outperforms the estimator in (5) and reduces the MSE of the channel estimation by 5.3% at high SNR. Even more remarkably, MSE'_p exactly matches $\text{MSE}_p^{\text{BLM}}$, which signifies that our proposed estimator achieves the same accuracy as the BLM estimator in (4) (see also Fig. 3(a)). In the following plots, we thus omit $\text{MSE}_p^{\text{BLM}}$, which allows us to evaluate scenarios with more UEs and longer pilots. A rigorous comparative analysis of our proposed estimator and

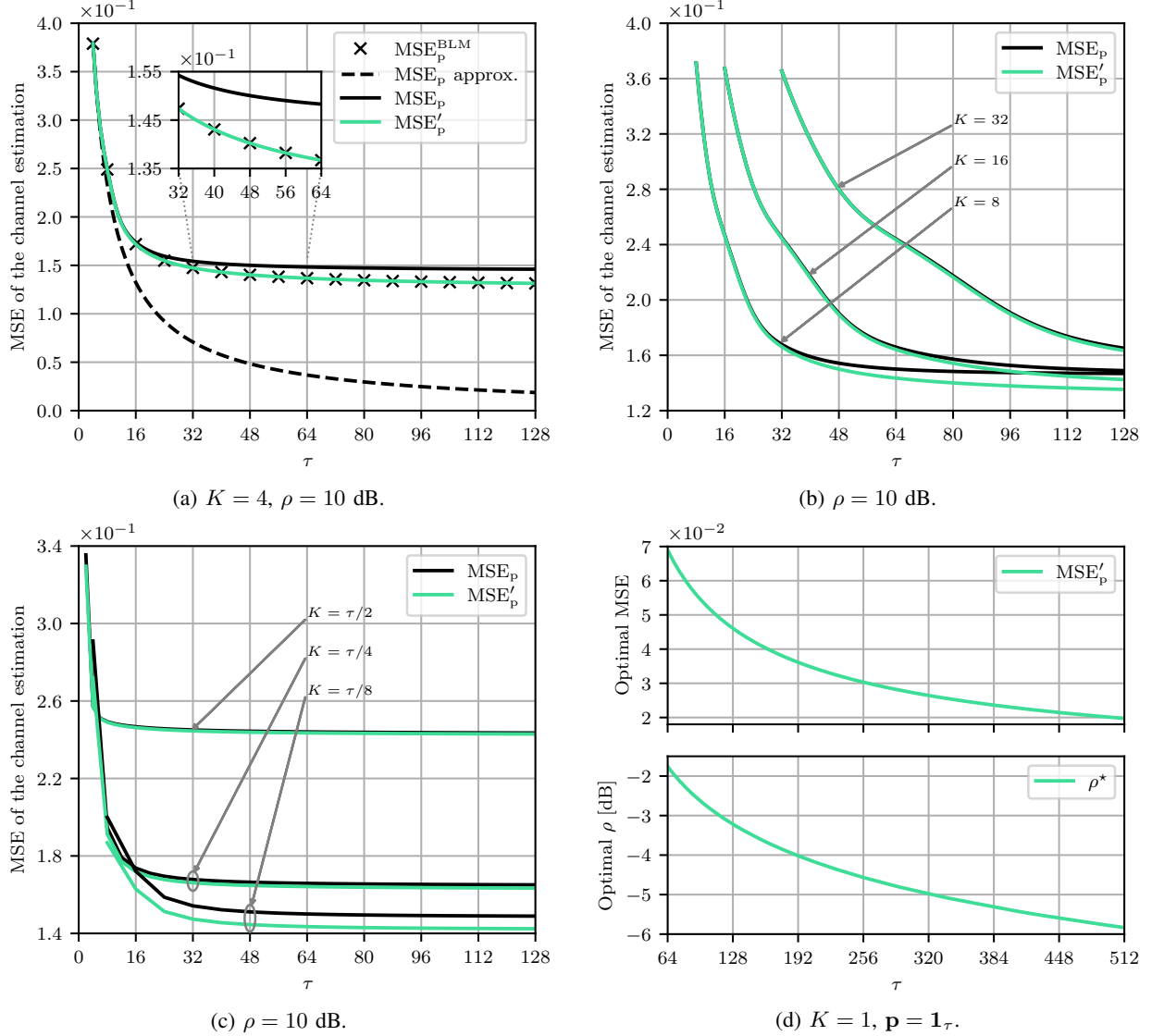


Fig. 3: MSE of the channel estimation against the pilot length.

the BLM estimator is left for future work. On the other hand, the approximated MSE expression in [9, Eq. (23)] proves to be highly unreliable even for $\rho < 0$ dB. Lastly, we highlight the SNR trade-off described in Sections III-A and III-B as well as in Appendix I, whereby the MSE of the channel estimation exhibits a valley at about $\rho = 3$ dB. Fig. 2(b) considers $\tau = 128$ and different values of K . Here, the gap between MSE'_p and MSE_p widens as the K decreases, reaching 8.5% for $K = 8$ at high SNR. Moreover, the SNR trade-off appears more evident for small values of K . Fig. 2(c) considers the single-UE case, showing that the upper bounds in (26) and (29) obtained by fixing $\mathbf{p} = \mathbf{1}_\tau$ are remarkably tight at low SNR and up to the region around the optimal transmit SNR. Note that the optimal value of ρ with $\mathbf{p} = \mathbf{1}_\tau$ satisfies the condition in (32) and gives an accurate approximation of the optimal value of ρ with $\mathbf{p} = \mathbf{d}_2$.

Fig. 3 plots the MSE of the channel estimation against the pilot length τ . The transmit SNR is fixed to $\rho = 10$ dB in Fig. 3(a)–(c), whereas Fig. 3(d) considers the optimized transmit SNR (we recall that ρ should be reduced as τ increases to enhance the channel estimation accuracy). Fig. 3(a) considers $K = 4$, where such a modest number of UEs allows us to evaluate the BLM estimator in (4) as well. We first observe that our proposed estimator in (17) reduces the MSE of the channel estimation with respect to the estimator in (5) by 10% for $\tau = 128$. Additionally, as in Fig. 2(a), MSE'_p exactly matches $\text{MSE}_p^{\text{BLM}}$, which means that our proposed estimator achieves the same accuracy as the BLM estimator. On the other hand, the approximated MSE expression in [9, Eq. (23)] proves to be highly unreliable as the gap with the exact expression increases with $\tau - K$. Fig. 3(b) considers different values of K , showing that the gap between MSE'_p and MSE_p widens as K decreases and reaches 7.8% for $K = 8$ and $\tau = 128$. Fig. 3(c) and examines the case where the number of UEs grows together with the pilot length. In this setting, the gap between MSE'_p and MSE_p is roughly constant and increases with the ratio $\frac{\tau}{K}$, reaching about 5% for $\frac{\tau}{K} = 8$. Lastly, Fig. 3(d) considers the single-UE case and the upper bound on MSE'_p in (29) obtained by fixing $\mathbf{p} = \mathbf{1}_\tau$, which is optimized over the transmit SNR for each τ . As discussed in Section III-B, the optimal value of ρ satisfies the condition in (32) and decreases as τ increases.

IV. DATA DECODING WITH 1-BIT ADCS AND MRC

In this section, we are interested in characterizing the performance of the data decoding with respect to the different parameters when 1-bit ADCs are adopted at each BS antenna (see Section II-B). In this regard, we consider the scenario where the BS uses our proposed estimator in (17) in the channel estimation phase and the MRC receiver in the data decoding phase. Under these assumptions, the combining matrix is given by $\mathbf{V} = \hat{\mathbf{H}}$ and we can rewrite (9) as

$$\hat{\mathbf{x}} = \sqrt{\Psi'} \mathbf{P}^H \mathbf{R}_p^H \mathbf{r} \quad (37)$$

$$\begin{aligned} &= \frac{\rho + 1}{2} \sqrt{\Psi'} \mathbf{P}^H \left(\text{sgn}(\text{Re}[\sqrt{\rho} \mathbf{H} \mathbf{P}^H + \mathbf{Z}_p]) + j \text{sgn}(\text{Im}[\sqrt{\rho} \mathbf{H} \mathbf{P}^H + \mathbf{Z}_p]) \right)^H \\ &\quad \times \left(\text{sgn}(\text{Re}[\sqrt{\rho} \mathbf{H} \mathbf{x} + \mathbf{z}]) + j \text{sgn}(\text{Im}[\sqrt{\rho} \mathbf{H} \mathbf{x} + \mathbf{z}]) \right) \end{aligned} \quad (38)$$

with Ψ' defined in (18). In the following, we focus on the single-UE case (i.e., $K = 1$) and characterize the statistical properties of the estimated symbols. Note that, in a multi-UE massive MIMO context with infinite-resolution ADCs, MRC asymptotically becomes the optimal receive strategy as the number of BS antennas increases. However, when the MRC receiver results from the quantized channel estimation, it cannot be perfectly aligned with the channel matrix, resulting

in residual multi-UE interference. Hence, the following analysis of the single-UE case does not consider this interference; nonetheless, the latter can be straightforwardly included at the expense of more involved and less insightful expressions.

A. Expected Value and Variance of the Estimated Symbols

Let $x \in \mathcal{S}$ be the transmit symbol of the UE, where $\mathcal{S} \triangleq \{s_1, \dots, s_L\}$ denotes the set of transmit symbols, with $s_\ell \in \mathbb{C}$, $\forall \ell$ (for instance, \mathcal{S} may correspond to the QPSK or 16-QAM constellation). To facilitate the data decoding process at the BS, for each transmit symbol $s_\ell \in \mathcal{S}$, we are interested in deriving the closed-form expression of the expected value of the resulting estimated symbol \hat{s}_ℓ .

Theorem 3. Assuming $K = 1$ and MRC, for each transmit symbol $s_\ell \in \mathcal{S}$, the expected value of the resulting estimated symbol \hat{s}_ℓ , denoted by $E_\ell \triangleq \mathbb{E}[\hat{s}_\ell]$, is given by

$$E_\ell = \sqrt{\frac{2}{\pi}} \rho M \frac{\tau}{\tau + \Delta} \sum_{u=1}^{\tau} p_u^* \left(\Omega \left(\frac{\rho \operatorname{Re}[p_u s_\ell]}{\sqrt{(\rho+1)(\rho|s_\ell|^2+1)}} \right) + j \Omega \left(\frac{\rho \operatorname{Im}[p_u s_\ell]}{\sqrt{(\rho+1)(\rho|s_\ell|^2+1)}} \right) \right) \quad (39)$$

with Δ defined in (15), which can be simplified for $K = 1$ as

$$\Delta = \sum_{u \neq v} \left(\operatorname{Re}[p_u^* p_v] \Omega \left(\frac{\rho \operatorname{Re}[p_u p_v^*]}{\rho + 1} \right) - \operatorname{Im}[p_u^* p_v] \Omega \left(\frac{\rho \operatorname{Im}[p_u p_v^*]}{\rho + 1} \right) \right). \quad (40)$$

Proof: See Appendix V. ■

The result of Theorem 3 can be exploited to efficiently implement MLD. In this context, each estimated symbol \hat{x} resulting from transmitting $x \in \mathcal{S}$ can be readily mapped to one of the expected values $\{E_1, \dots, E_L\}$ derived as in (39) without any prior Monte Carlo computation of the latter. To further simplify the process and avoid computing the distance between \hat{x} and each E_ℓ , one can construct the Voronoi tessellation based on $\{E_1, \dots, E_L\}$ (and possibly other available information) obtaining well-defined decoding regions.

Now, for each transmit symbol $s_\ell \in \mathcal{S}$, we derive the closed-form expression of the variance of the resulting estimated symbol \hat{s}_ℓ .

Theorem 4. Assuming $K = 1$ and MRC, for each transmit symbol $s_\ell \in \mathcal{S}$, the variance of the resulting estimated symbol \hat{s}_ℓ , denoted by $V_\ell \triangleq \mathbb{V}[\hat{s}_\ell]$, is given by

$$V_\ell = \frac{2}{\pi} \rho M \frac{\tau^2}{\tau + \Delta} - \frac{1}{M} |E_\ell|^2 \quad (41)$$

with Δ given in (40) and where E_ℓ is derived in closed form in (39).

Proof: See Appendix VI. ■

The result of Theorem 4 quantifies the dispersion of the estimated symbols about their expected value, which results from the 1-bit quantization applied to both the channel estimation (through the MRC receiver) and the data decoding. This dispersion is not isotropic and assumes different shapes for different transmit symbols, as illustrated in Section IV-C. Some additional comments are in order. Firstly, V_ℓ reduces as $|s_\ell|$ increases due to the negative term on the right-hand side of (41): this is somewhat intuitive since the transmit symbols that lie further from the origin are less subject to noise. Secondly, although V_ℓ increases linearly with the number of BS antennas M , the normalized variance $\frac{V_\ell}{|E_\ell|^2}$ (which expresses the relative dispersion of the estimated symbols about their expected value) is inversely proportional to M . Thirdly, the combined results of Theorems 3 and 4 can be exploited to design the set of transmit symbols \mathcal{S} by jointly minimizing the relative dispersion and the overlap between different symbols after the estimation (this is left for future work). Lastly, in the context of MLD via Voronoi tessellation described above, one can use the variance derived as in (41) to further refine the decoding regions.

It is of particular interest to study the asymptotic behavior of the expected value and variance of the estimated symbols at high SNR.

Corollary 2. From Theorems 3 and 4, in the limit of $\rho \rightarrow \infty$, we have

$$\lim_{\rho \rightarrow \infty} \frac{E_\ell}{\sqrt{\rho}} = \sqrt{\frac{2}{\pi}} M \frac{\tau}{\tau + \bar{\Delta}} \sum_{u=1}^{\tau} p_u^* \left(\Omega \left(\frac{\text{Re}[p_u s_\ell]}{|s_\ell|} \right) + j \Omega \left(\frac{\text{Im}[p_u s_\ell]}{|s_\ell|} \right) \right) \quad (42)$$

and

$$\lim_{\rho \rightarrow \infty} \frac{V_\ell}{\rho} = \frac{2}{\pi} M \frac{\tau^2}{\tau + \bar{\Delta}} - \frac{1}{M} \lim_{\rho \rightarrow \infty} \frac{|E_\ell|^2}{\rho} \quad (43)$$

with $\bar{\Delta}$ defined in (24), which can be simplified for $K = 1$ as

$$\bar{\Delta} = \sum_{u \neq v} \left(\text{Re}[p_u^* p_v] \Omega(\text{Re}[p_u p_v^*]) - \text{Im}[p_u^* p_v] \Omega(\text{Im}[p_u p_v^*]) \right). \quad (44)$$

Corollary 2 formalizes a behavior of the estimated symbols that was observed in [9]. From (42), it emerges that, at high SNR, all the estimated symbols lie on a circle around the origin and their amplitude no longer conveys any information. As a consequence, the estimated symbols resulting from transmit symbols with the same phase become indistinguishable in terms of their expected value, which depends only on $\frac{\text{Re}[s_\ell]}{|s_\ell|}$ and $\frac{\text{Im}[s_\ell]}{|s_\ell|}$. For instance, if \mathcal{S} corresponds to the 16-QAM constellation as in Section IV-C, the inner estimated symbols become indistinguishable from the outer estimated symbols with the same phase. Furthermore, according to (43), these estimated symbols become identical also in terms of variance. In the light of this, blindly minimizing

the (normalized) variance of the estimated symbols is not the key to enhancing the system performance. Instead, the variance (which roughly decreases with the transmit SNR) should be minimized alongside the overlap between different symbols after the estimation (which generally increases with the transmit SNR). This determines a clear SNR trade-off, according to which operating at the right noise level enhances the data decoding accuracy and thus reduces the SER.

B. Tractable Upper Bounds

As done in Section III-B for the MSE of the channel estimation, tractable upper bounds on the normalized variance of the estimated symbols (i.e., that do not depend on the specific pilot choice) can be obtained by fixing $\mathbf{p} = \mathbf{1}_\tau$, since such a structure of \mathbf{p} represents the worst possible pilot choice (see Appendix I). Hence, plugging (25) into (41) and (43) yields

$$\begin{aligned} \frac{V_\ell}{|E_\ell|^2} = & \frac{1}{M} \frac{1 + (\tau - 1)\Omega\left(\frac{\rho}{\rho+1}\right)}{\tau} \left(\left(\Omega\left(\frac{\rho \text{Re}[s_\ell]}{\sqrt{(\rho+1)(\rho|s_\ell|^2+1)}}\right) \right)^2 \right. \\ & \left. + \left(\Omega\left(\frac{\rho \text{Im}[s_\ell]}{\sqrt{(\rho+1)(\rho|s_\ell|^2+1)}}\right) \right)^2 \right)^{-1} - \frac{1}{M} \end{aligned} \quad (45)$$

and

$$\lim_{\rho \rightarrow \infty} \frac{V_\ell}{|E_\ell|^2} = \frac{1}{M} \left(\left(\Omega\left(\frac{\text{Re}[s_\ell]}{|s_\ell|}\right) \right)^2 + \left(\Omega\left(\frac{\text{Im}[s_\ell]}{|s_\ell|}\right) \right)^2 \right)^{-1} - \frac{1}{M} \quad (46)$$

respectively. In addition, considering (45) in the limit of $\tau \rightarrow \infty$, we have

$$\begin{aligned} \lim_{\tau \rightarrow \infty} \frac{V_\ell}{|E_\ell|^2} = & \frac{1}{M} \Omega\left(\frac{\rho}{\rho+1}\right) \left(\left(\Omega\left(\frac{\rho \text{Re}[s_\ell]}{\sqrt{(\rho+1)(\rho|s_\ell|^2+1)}}\right) \right)^2 \right. \\ & \left. + \left(\Omega\left(\frac{\rho \text{Im}[s_\ell]}{\sqrt{(\rho+1)(\rho|s_\ell|^2+1)}}\right) \right)^2 \right)^{-1} - \frac{1}{M}. \end{aligned} \quad (47)$$

Some comments are in order. Firstly, the normalized variance of the estimated symbols can be made arbitrarily close to zero by increasing the number of BS antennas M . Secondly, (46) does not depend on τ since, in the absence of noise, estimating the channel repeatedly over the same pilot symbol does not bring any benefit. Thirdly, it can be shown that (45) is a quasiconvex function of ρ and, as such, it has a unique minimum that defines a further SNR trade-off. It is shown in Section IV-C that this SNR trade-off, which is inherited from the channel estimation phase through the MRC receiver, is not as significant as that described by Corollary 2. In fact, the normalized variance of the estimated symbols roughly decreases with ρ ; on the other hand, the difference in amplitude between symbols cannot be recovered if ρ is too high. Lastly, we point out that the system performance can be further enhanced by optimizing the transmit SNR separately for the two phases of channel estimation and uplink data transmission.

C. Numerical Results and Discussion

We now focus on the performance evaluation of the data decoding with 1-bit ADCs with respect to the different parameters using the analytical results presented in Sections IV-A and IV-B. In this regard, we assume that the BS uses our proposed estimator in (17) in the channel estimation phase and the MRC receiver in the data decoding phase. We thus consider the expressions of E_ℓ and V_ℓ derived in (39) and (41), respectively, for the single-UE case (i.e., $K = 1$). As in Section III-C, we use the pilots $\mathbf{p} = \mathbf{d}_2$, with \mathbf{d}_2 defined in (33), and $\mathbf{p} = \mathbf{1}_\tau$. Moreover, we specifically analyze the scenario where the set of transmit symbols \mathcal{S} corresponds to the 16-QAM constellation, i.e., $\mathcal{S} = \frac{1}{\sqrt{10}}\{\pm 1 \pm j, \pm 1 \pm j3, \pm 3 \pm j, \pm 3 \pm j3\}$, which is normalized such that $\frac{1}{L} \sum_{\ell=1}^L |s_\ell|^2 = 1$; however, we remark that our analytical framework is valid for any choice of \mathcal{S} .

Fig. 4 plots the estimated symbols for different settings, where each 16-QAM symbol is transmitted over 10^2 independent channel realizations and $\mathbf{p} = \mathbf{d}_2$ is used in the channel estimation phase. The expected value of the estimated symbols is computed as in Theorem 3: this matches the sample average of the estimated symbols for each 16-QAM transmit symbol and can be used to efficiently implement MLD. Comparing Fig. 4(a)–(c), which consider the same transmit SNR and pilot length, the relative dispersion of the estimated symbols about their expected value reduces as the number of BS antennas grows from $M = 64$ to $M = 256$. In fact, a higher granularity in the antenna domain allows to sum the contribution of a larger number of independent channel entries. On the other hand, comparing Fig. 4(b) and (d), which consider the same number of BS antennas and transmit SNR, the relative dispersion of the estimated symbols about their expected value slightly intensifies as we decrease the pilot length from $\tau = 32$ to $\tau = 8$. This stems from the overall diminished accuracy of the channel estimate used to compute the MRC receiver for each channel realization. Lastly, comparing Fig. 4(b) and (e)–(f), which consider the same number of BS antennas and pilot length, the estimated symbols resulting from the 16-QAM transmit symbols with the same phase, i.e., $\pm \frac{1}{\sqrt{10}}(1 \pm j)$ and $\pm \frac{1}{\sqrt{10}}(3 \pm j3)$, get closer as the transmit SNR increases from $\rho = 0$ dB to $\rho = 10$ dB and they almost fully overlap for $\rho = 20$ dB. This behavior was observed in [9] and is formalized in Corollary 2, according to which such estimated symbols become identical in terms of both their expected value and variance at high SNR. In this respect, the SNR trade-off described in Sections IV-A and IV-B is quite evident: while the normalized variance of the estimated symbols roughly decreases with ρ , the difference in amplitude between symbols cannot be recovered if ρ is too high. For the 16-

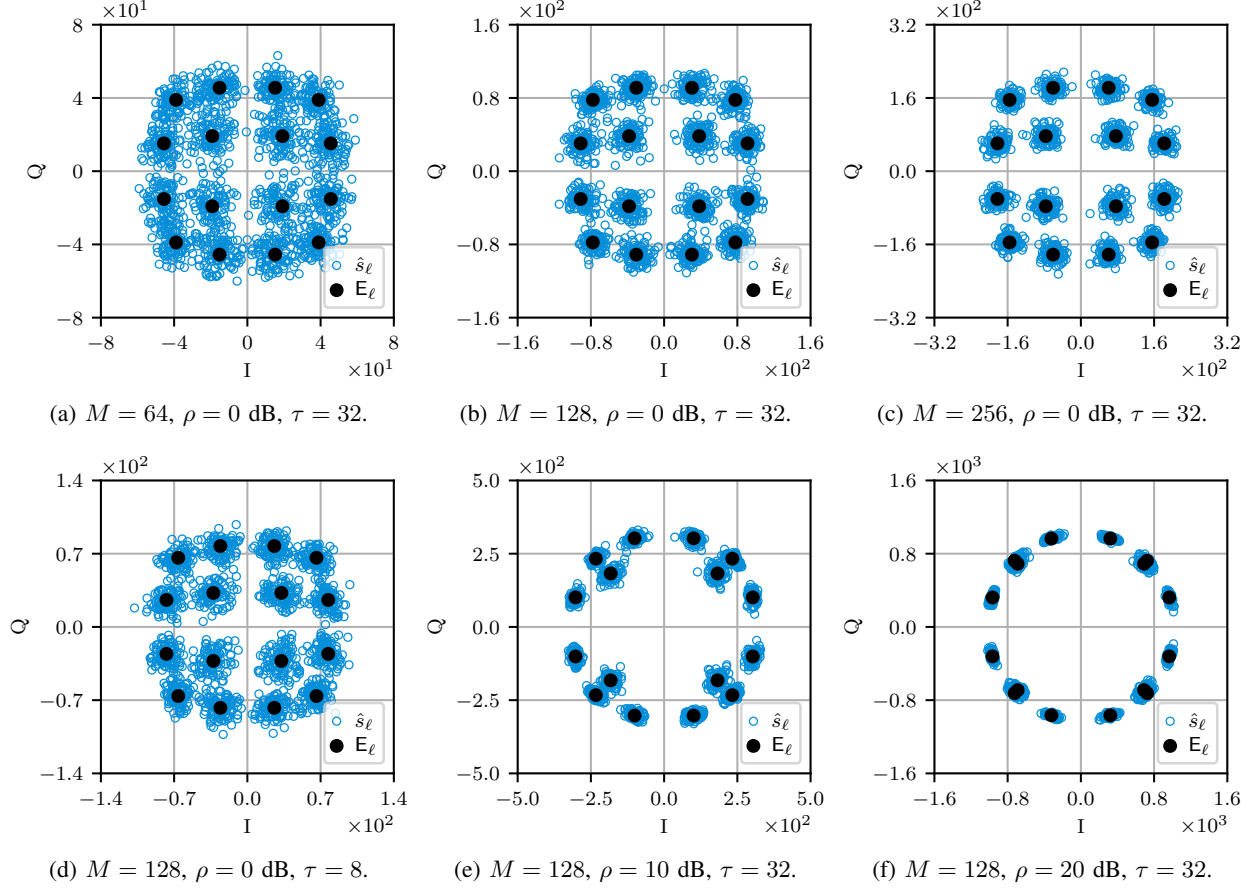


Fig. 4: Estimated symbols with the MRC receiver, with 16-QAM transmit symbols and $K = 1$. The expected value of the estimated symbols is computed as in (39).

QAM, this produces a SER of about 25% since there are four pairs of indistinguishable estimated symbols (see also Fig. 8). In summary, having independent phases between the channel entries and operating at the right noise level are crucial to accurately estimate the phases and the amplitudes, respectively; we refer to Appendix I and to the related discussion in [9] for more details.

Let us now examine the behavior of the variance of the estimated symbols derived in Theorem 4. Fig. 5 considers $\rho = 10 \text{ dB}$ and $\tau = 32$, showing how the normalized variance of the estimated symbols $\frac{V_\ell}{|E_\ell|^2}$ decreases with the number of BS antennas M . The transmit symbols $\pm \frac{1}{\sqrt{10}}(1 \pm j)$, having the smallest power among the 16-QAM constellation, exhibit the most severe dispersion of the estimated symbols about their expected value. Furthermore, the upper bound in (45) becomes more accurate as M grows. Fig. 6 considers $M = 128$ and $\tau = 32$, showing that $\frac{V_\ell}{|E_\ell|^2}$ generally diminishes with the transmit SNR ρ except for the SNR trade-off exhibited with $\mathbf{p} = \mathbf{1}_\tau$ at about $\rho = 10 \text{ dB}$; here, the asymptotic expressions in (43) and (46) are also included. Despite this trend, we recall that the difference in amplitude between symbols cannot be recovered if

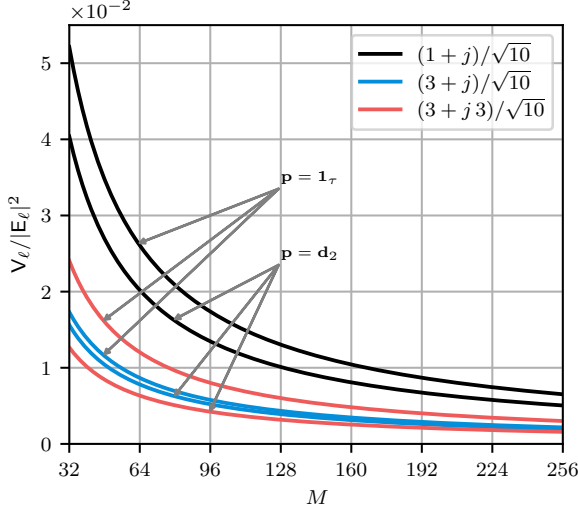


Fig. 5: Normalized variance of the estimated symbols against the number of BS antennas, with 16-QAM transmit symbols, $K = 1$, $\rho = 10$ dB, and $\tau = 32$.

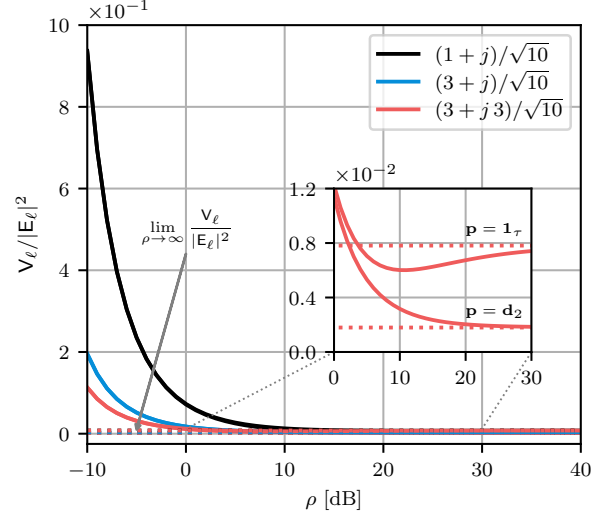


Fig. 6: Normalized variance of the estimated symbols against the transmit SNR, with 16-QAM transmit symbols, $K = 1$, $M = 128$, and $\tau = 32$.

ρ is too high, as discussed in the previous paragraph for Fig. 4: thus, arbitrarily increasing the transmit SNR is detrimental for the system performance. Lastly, Fig. 7 considers $M = 128$ and $\rho = 10$ dB, showing how $\frac{V_\ell}{|E_\ell|^2}$ reduces with the pilot length τ .

We conclude this section by investigating the combined impact of the channel estimation and the data decoding with 1-bit ADCs on the system performance in terms of SER, which we compute numerically via Monte Carlo simulations with 10^6 independent channel realizations. In this context, the symbols are decoded by means of MLD aided by the result of Theorem 3. Fig. 8 illustrates the SER against the transmit SNR ρ , with $M = 128$ and $\tau = 32$. Here, the SNR trade-off appears quite evident, whereby the SER decreases until it reaches its minimum at about $\rho = 5$ dB (where the upper bound obtained with $\mathbf{p} = \mathbf{1}_\tau$ proves to be remarkably tight) before escalating again. Then, the SER asymptotically reaches 25% at high SNR, where the inner estimated symbols of the 16-QAM constellation become indistinguishable from the outer estimated symbols with the same phase (see also Fig. 4(f)). We remark that the SER can be further reduced by optimizing the transmit SNR separately for the two phases of channel estimation and uplink data transmission, which is left for future work.

V. CONCLUSIONS

This paper presents an analytical framework for the channel estimation and the data decoding in massive MIMO uplink systems with 1-bit ADCs. First, we provide a precise characterization of the MSE of the channel estimation with respect to different parameters and additionally propose a novel linear estimator with significantly enhanced performance compared with existing estimators

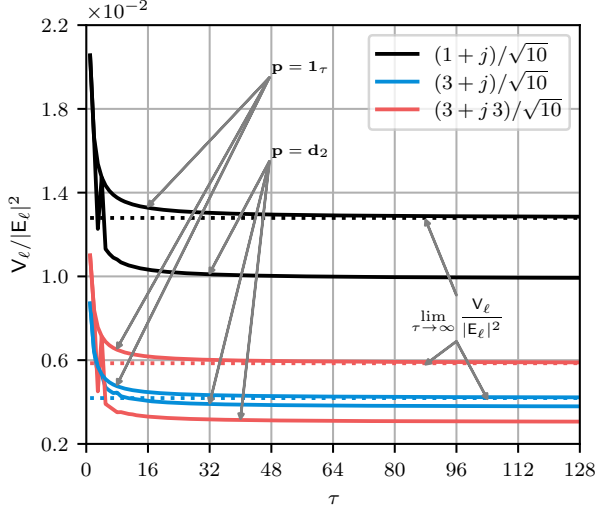


Fig. 7: Normalized variance of the estimated symbols against the pilot length, with 16-QAM transmit symbols, $K = 1$, $M = 128$, and $\rho = 10$ dB.

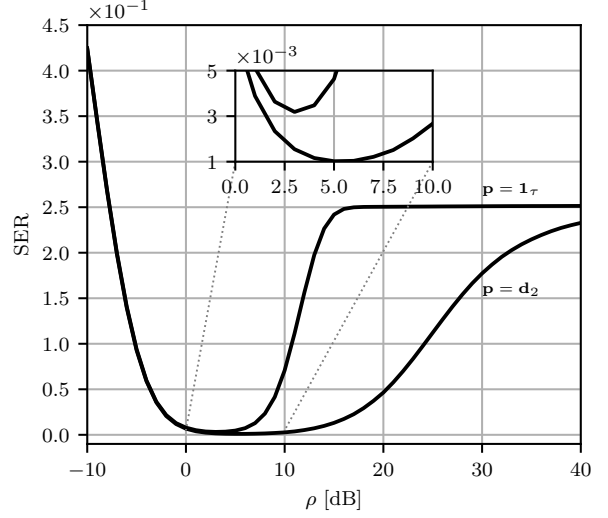


Fig. 8: SER against the transmit SNR, with 16-QAM transmit symbols, $K = 1$, $M = 128$, and $\tau = 32$.

with the same structure. For the data decoding, we characterize the expected value and the variance of the estimated symbols when MRC is adopted, which can be exploited to efficiently implement MLD and to properly design the set of transmit symbols. The proposed analysis gives important practical insights into the design and the implementation of 1-bit quantized systems. In particular, it highlights a fundamental SNR trade-off, according to which arbitrarily increasing the transmit SNR is detrimental for the system performance. In this respect, the optimal transmit SNR for the channel estimation is shown to decrease as the pilot length increases. Future work will consider a rigorous comparative analysis between our proposed estimator and the BLM estimator, extensions of the proposed analytical framework to more realistic channel models, and a SER optimal design of the set of transmit symbols capitalizing on our data decoding analysis.

APPENDIX I

FUNDAMENTALS OF CHANNEL ESTIMATION WITH 1-BIT ADCS

Assuming $K = 1$, let $\mathbf{h} \triangleq (h_m) \in \mathbb{C}^{M \times 1}$ and $\mathbf{p} \triangleq (p_u) \in \mathbb{C}^{\tau \times 1}$ denote the uplink channel vector and the pilot, respectively, of the UE. When an estimator with the structure of (5) is used, the channel estimate $\hat{\mathbf{h}} \triangleq (\hat{h}_m)$ is obtained as

$$\hat{\mathbf{h}} = \sqrt{\Psi}Q \left(\begin{bmatrix} \sqrt{\rho}h_1p_1^* + Z_{1,1} & \cdots & \sqrt{\rho}h_1p_\tau^* + Z_{1,\tau} \\ \vdots & \ddots & \vdots \\ \sqrt{\rho}h_Mp_1^* + Z_{M,1} & \cdots & \sqrt{\rho}h_Mp_\tau^* + Z_{M,\tau} \end{bmatrix} \right) \begin{bmatrix} p_1 \\ \vdots \\ p_\tau \end{bmatrix} \quad (48)$$

with

$$\hat{h}_m = \sqrt{\frac{\rho+1}{2}} \Psi \sum_{u=1}^{\tau} p_u \left(\text{sgn}(\text{Re}[\sqrt{\rho} h_m p_u^* + Z_{m,u}]) + j \text{sgn}(\text{Im}[\sqrt{\rho} h_m p_u^* + Z_{m,u}]) \right). \quad (49)$$

The phase of each channel entry h_m can be estimated with improved accuracy as the pilot length increases, provided that the entries of \mathbf{p} span the unit circle as much as possible. In this regard, the best pilot choice is given by the second column of the τ -dimensional DFT matrix defined in (33), since its entries are non-repeating and equispaced on the unit circle; on the contrary, the worst pilot choice is given by fixing \mathbf{p} such that $p_u \in \{\pm\beta, \pm j\beta\}$, $\forall u$, where $\beta \in \mathbb{C}$ and $|\beta|^2 = 1$ (a simple choice is $\mathbf{p} = \mathbf{1}_\tau$). On the other hand, the estimation of the amplitude of h_m benefits from operating at the right noise level, as we will see next.

Let $h_m = \alpha_m e^{j\theta_m}$, with $\vartheta_m \triangleq (\theta_m \bmod \frac{\pi}{2})$, and let $p_u = e^{j\phi_u}$ (recall that $|p_u|^2 = 1$, $\forall u$). Assuming $\rho \rightarrow \infty$, the phase of h_m can be estimated from $Q(h_m \mathbf{p}^H) \mathbf{p}$, where

$$Q(h_m p_u^*) p_u = Q(e^{j(\theta_m - \phi_u)}) e^{j\phi_u} \quad (50)$$

$$= \begin{cases} \sqrt{\frac{\rho+1}{2}} (\text{sgn}(\text{Re}[h_m]) + j \text{sgn}(\text{Im}[h_m])) e^{j\phi_u} & \text{if } \phi_u \in [\vartheta_m - \frac{\pi}{2}, \vartheta_m], \\ \sqrt{\frac{\rho+1}{2}} (\text{sgn}(\text{Im}[h_m]) - j \text{sgn}(\text{Re}[h_m])) e^{j\phi_u} & \text{if } \phi_u \in [\vartheta_m, \vartheta_m + \frac{\pi}{2}], \\ \sqrt{\frac{\rho+1}{2}} (-\text{sgn}(\text{Re}[h_m]) - j \text{sgn}(\text{Im}[h_m])) e^{j\phi_u} & \text{if } \phi_u \in [\vartheta_m + \frac{\pi}{2}, \vartheta_m + \pi], \\ \sqrt{\frac{\rho+1}{2}} (-\text{sgn}(\text{Im}[h_m]) + j \text{sgn}(\text{Re}[h_m])) e^{j\phi_u} & \text{if } \phi_u \in [\vartheta_m + \pi, \vartheta_m + \frac{3\pi}{2}] \end{cases} \quad (51)$$

i.e., $Q(e^{j(\theta_m - \phi_u)})$ shifts quadrant according to the phase of p_u . Assuming that the entries of \mathbf{p} span the unit circle, in the limit of $\tau \rightarrow \infty$, we have

$$\begin{aligned} \lim_{\tau \rightarrow \infty} \frac{1}{\tau} \sum_{u=1}^{\tau} Q(h_m p_u^*) p_u &= \frac{1}{2\pi} \sqrt{\frac{\rho+1}{2}} \left((\text{sgn}(\text{Re}[h_m]) + j \text{sgn}(\text{Im}[h_m])) \int_{\vartheta_m - \frac{\pi}{2}}^{\vartheta_m} e^{j\phi} d\phi \right. \\ &\quad + (\text{sgn}(\text{Im}[h_m]) - j \text{sgn}(\text{Re}[h_m])) \int_{\vartheta_m}^{\vartheta_m + \frac{\pi}{2}} e^{j\phi} d\phi \\ &\quad + (-\text{sgn}(\text{Re}[h_m]) - j \text{sgn}(\text{Im}[h_m])) \int_{\vartheta_m + \frac{\pi}{2}}^{\vartheta_m + \pi} e^{j\phi} d\phi \\ &\quad \left. + (-\text{sgn}(\text{Im}[h_m]) + j \text{sgn}(\text{Re}[h_m])) \int_{\vartheta_m + \pi}^{\vartheta_m + \frac{3\pi}{2}} e^{j\phi} d\phi \right) \quad (52) \end{aligned}$$

$$= \frac{2}{\pi} \sqrt{\frac{\rho+1}{2}} (1-j) (\text{sgn}(\text{Re}[h_m]) + j \text{sgn}(\text{Im}[h_m])) e^{j\vartheta_m} \quad (53)$$

where (53) follows from

$$\int_{\vartheta_m - \frac{\pi}{2}}^{\vartheta_m} e^{j\phi} d\phi = (1-j) e^{j\vartheta_m}, \quad \int_{\vartheta_m}^{\vartheta_m + \frac{\pi}{2}} e^{j\phi} d\phi = (1+j) e^{j\vartheta_m}, \quad (54)$$

$$\int_{\vartheta_m + \frac{\pi}{2}}^{\vartheta_m + \pi} e^{j\phi} d\phi = (-1+j) e^{j\vartheta_m}, \quad \int_{\vartheta_m + \pi}^{\vartheta_m + \frac{3\pi}{2}} e^{j\phi} d\phi = (-1-j) e^{j\vartheta_m}. \quad (55)$$

Finally, from (53), we have

$$(1-j)\left(\text{sgn}(\text{Re}[h_m]) + j \text{sgn}(\text{Im}[h_m])\right) e^{j\vartheta_m} \\ = \begin{cases} 2e^{j\vartheta_m} & \text{if } \theta_m \in [0, \frac{\pi}{2}] \text{ (i.e., if } \theta_m = \vartheta_m), \\ 2j e^{j\vartheta_m} & \text{if } \theta_m \in [\frac{\pi}{2}, \pi] \text{ (i.e., if } \theta_m = \vartheta_m + \frac{\pi}{2}), \\ -2e^{j\vartheta_m} & \text{if } \theta_m \in [\pi, \frac{3\pi}{2}] \text{ (i.e., if } \theta_m = \vartheta_m + \pi), \\ -2j e^{j\vartheta_m} & \text{if } \theta_m \in [\frac{3\pi}{2}, 2\pi] \text{ (i.e., if } \theta_m = \vartheta_m + \frac{3\pi}{2}) \end{cases} \quad (56)$$

$$= 2e^{j\theta_m} \quad (57)$$

which gives

$$\lim_{\tau \rightarrow \infty} \frac{1}{\tau} \sum_{u=1}^{\tau} Q(h_m p_u^*) p_u = \frac{4}{\pi} \sqrt{\frac{\rho+1}{2}} e^{j\theta_m}. \quad (58)$$

Hence, the phase of h_m can be estimated accurately if the pilot symbols span the unit circle and τ is sufficiently large. However, (58) does not include any information about the amplitude due to the assumption that $\rho \rightarrow \infty$.

Assuming now finite ρ and, for simplicity, $\mathbf{p} = \mathbf{1}_\tau$, the amplitude of h_m can be estimated from $Q(\sqrt{\rho}h_m \mathbf{1}_\tau^T + [Z_{m,1}, \dots, Z_{m,\tau}]) \mathbf{1}_\tau$, where

$$Q(\sqrt{\rho}h_m + Z_{m,u}) = \sqrt{\frac{\rho+1}{2}} \left(\text{sgn}(\sqrt{\rho}\text{Re}[h_m] + \text{Re}[Z_{m,u}]) + j \text{sgn}(\sqrt{\rho}\text{Im}[h_m] + \text{Im}[Z_{m,u}]) \right). \quad (59)$$

In the limit of $\tau \rightarrow \infty$, we have

$$\lim_{\tau \rightarrow \infty} \frac{1}{\tau} \sum_{u=1}^{\tau} Q(\sqrt{\rho}h_m + Z_{m,u}) = \sqrt{\frac{\rho+1}{2}} \left(\text{erf}(\sqrt{\rho}\text{Re}[h_m]) + j \text{erf}(\sqrt{\rho}\text{Im}[h_m]) \right) \quad (60)$$

where $\text{erf}(w) \triangleq \frac{2}{\sqrt{\pi}} \int_0^w e^{-t^2} dt$ denotes the error function. Since $\text{erf}(w)$ is approximately linear for $w \in [-1, 1]$, the difference in amplitude between channel entries can be estimated accurately if their real and imaginary parts lie in $[-\frac{1}{\sqrt{\rho}}, \frac{1}{\sqrt{\rho}}]$ and τ is sufficiently large (a similar conclusion can be drawn for $\mathbf{p} \neq \mathbf{1}_\tau$). On the other hand, if τ is not sufficiently large at low SNR, the channel estimates are corrupted by the strong noise. Hence, the SNR plays an important role since operating at the right noise level significantly enhances the channel estimation accuracy.

APPENDIX II

PROOF OF PROPOSITION 1

To obtain the expression in (10), we first observe that

$$\mathbb{E}[\text{sgn}(X_1)\text{sgn}(X_2)] = \mathbb{P}[X_1 > 0, X_2 > 0] + \mathbb{P}[X_1 < 0, X_2 < 0] \\ - \mathbb{P}[X_1 > 0, X_2 < 0] - \mathbb{P}[X_1 < 0, X_2 > 0]. \quad (61)$$

For $X_1 = \mathbf{a}_1^T \boldsymbol{\zeta}$ and $X_2 = \mathbf{a}_2^T \boldsymbol{\zeta}$, the first term on the right-hand side of (61) can be obtained building on [27] as

$$\mathbb{P}[\mathbf{a}_1^T \boldsymbol{\zeta} > 0, \mathbf{a}_2^T \boldsymbol{\zeta} > 0] = \frac{1}{4} \left(1 + \Omega \left(\frac{\mathbf{a}_1^T \mathbf{a}_2}{\|\mathbf{a}_1\| \|\mathbf{a}_2\|} \right) \right) \quad (62)$$

where $\frac{\mathbf{a}_1^T \mathbf{a}_2}{\|\mathbf{a}_1\| \|\mathbf{a}_2\|}$ represents the correlation coefficient between X_1 and X_2 , and the other terms can be obtained following similar steps. ■

APPENDIX III

PROOF OF THEOREM 1

We begin by rewriting (12) as

$$\text{MSE}_p = \frac{1}{MK} \left(\mathbb{E}[\text{tr}(\mathbf{H}^H \mathbf{H})] + \mathbb{E}[\text{tr}(\hat{\mathbf{H}}^H \hat{\mathbf{H}})] - 2\mathbb{E}[\text{Re}[\text{tr}(\hat{\mathbf{H}}^H \mathbf{H})]] \right) \quad (63)$$

with $\mathbb{E}[\text{tr}(\mathbf{H}^H \mathbf{H})] = MK$. Next, we derive the second and third expectation terms of (63). To this end, we introduce the following definitions:

$$A_{m,u} \triangleq \text{sgn} \left(\text{Re} \left[\sqrt{\rho} \sum_{k=1}^K H_{m,k} P_{u,k}^* + Z_{m,u} \right] \right) \quad (64)$$

$$= \text{sgn} \left(\sqrt{\rho} \sum_{k=1}^K (\text{Re}[H_{m,k}] \text{Re}[P_{u,k}] + \text{Im}[H_{m,k}] \text{Im}[P_{u,k}]) + \text{Re}[Z_{m,u}] \right), \quad (65)$$

$$B_{m,u} \triangleq \text{sgn} \left(\text{Im} \left[\sqrt{\rho} \sum_{k=1}^K H_{m,k} P_{u,k}^* + Z_{m,u} \right] \right) \quad (66)$$

$$= \text{sgn} \left(\sqrt{\rho} \sum_{k=1}^K (-\text{Re}[H_{m,k}] \text{Im}[P_{u,k}] + \text{Im}[H_{m,k}] \text{Re}[P_{u,k}]) + \text{Im}[Z_{m,u}] \right). \quad (67)$$

- Considering the second expectation term in (63), we have

$$\text{tr}(\hat{\mathbf{H}}^H \hat{\mathbf{H}}) = \frac{\rho K + 1}{2} \Psi \sum_{m=1}^M \sum_{k=1}^K \left(\sum_{u=1}^{\tau} P_{u,k} (A_{m,u} + j B_{m,u}) \right)^* \left(\sum_{u=1}^{\tau} P_{u,k} (A_{m,u} + j B_{m,u}) \right) \quad (68)$$

$$= \frac{\rho K + 1}{2} \Psi \sum_{m=1}^M \sum_{k=1}^K \sum_{u=1}^{\tau} \sum_{v=1}^{\tau} P_{u,k}^* P_{v,k} (A_{m,u} A_{m,v} + B_{m,u} B_{m,v} + j (A_{m,u} B_{m,v} - B_{m,u} A_{m,v})) \quad (69)$$

$$= \frac{\rho K + 1}{2} \Psi \left(2MK\tau + \sum_{m=1}^M \sum_{k=1}^K \sum_{u \neq v} P_{u,k}^* P_{v,k} (A_{m,u} A_{m,v} + B_{m,u} B_{m,v} + j (A_{m,u} B_{m,v} - B_{m,u} A_{m,v})) \right). \quad (70)$$

Hence, the expected value of (70) is given by

$$\begin{aligned}\mathbb{E}[\text{tr}(\hat{\mathbf{H}}^H \hat{\mathbf{H}})] &= (\rho K + 1) \Psi M \left(K\tau + \sum_{k=1}^K \sum_{u \neq v} P_{u,k}^* P_{v,k} \left(\Omega \left(\frac{\rho \sum_{i=1}^K \text{Re}[P_{u,i} P_{v,i}^*]}{\rho K + 1} \right) \right. \right. \\ &\quad \left. \left. + j \Omega \left(\frac{\rho \sum_{i=1}^K \text{Im}[P_{u,i} P_{v,i}^*]}{\rho K + 1} \right) \right) \right) \\ &= (\rho K + 1) \Psi M \left(K\tau + \sum_{k=1}^K \sum_{u \neq v} \left(\text{Re}[P_{u,k}^* P_{v,k}] \Omega \left(\frac{\rho \sum_{i=1}^K \text{Re}[P_{u,i} P_{v,i}^*]}{\rho K + 1} \right) \right. \right. \\ &\quad \left. \left. - \text{Im}[P_{u,k}^* P_{v,k}] \Omega \left(\frac{\rho \sum_{i=1}^K \text{Im}[P_{u,i} P_{v,i}^*]}{\rho K + 1} \right) \right) \right) \end{aligned} \quad (71)$$

$$\begin{aligned} &= (\rho K + 1) \Psi M \left(K\tau + \sum_{k=1}^K \sum_{u \neq v} \left(\text{Re}[P_{u,k}^* P_{v,k}] \Omega \left(\frac{\rho \sum_{i=1}^K \text{Re}[P_{u,i} P_{v,i}^*]}{\rho K + 1} \right) \right. \right. \\ &\quad \left. \left. - \text{Im}[P_{u,k}^* P_{v,k}] \Omega \left(\frac{\rho \sum_{i=1}^K \text{Im}[P_{u,i} P_{v,i}^*]}{\rho K + 1} \right) \right) \right) \end{aligned} \quad (72)$$

where (71) follows from

$$\mathbb{E}[A_{m,u} A_{m,v}] = \mathbb{E}[B_{m,u} B_{m,v}] \quad (73)$$

$$= \Omega \left(\frac{\rho \sum_{k=1}^K \text{Re}[P_{u,k} P_{v,k}^*]}{\rho K + 1} \right), \quad (74)$$

$$\mathbb{E}[A_{m,u} B_{m,v}] = \Omega \left(\frac{\rho \sum_{k=1}^K \text{Im}[P_{u,k} P_{v,k}^*]}{\rho K + 1} \right) \quad (75)$$

which are derived by applying Proposition 1. For instance, $\mathbb{E}[A_{m,u} A_{m,v}]$ in (73)–(74) can be obtained by plugging

$$\boldsymbol{\zeta} = [\text{Re}[H_{m,1}], \dots, \text{Re}[H_{m,K}], \text{Im}[H_{m,1}], \dots, \text{Im}[H_{m,K}], \text{Re}[Z_{m,u}], \text{Re}[Z_{m,v}]]^T, \quad (76)$$

$$\mathbf{a}_1 = [\sqrt{\rho} \text{Re}[P_{u,1}], \dots, \sqrt{\rho} \text{Re}[P_{u,K}], \sqrt{\rho} \text{Im}[P_{u,1}], \dots, \sqrt{\rho} \text{Im}[P_{u,K}], 1, 0]^T, \quad (77)$$

$$\mathbf{a}_2 = [\sqrt{\rho} \text{Re}[P_{v,1}], \dots, \sqrt{\rho} \text{Re}[P_{v,K}], \sqrt{\rho} \text{Im}[P_{v,1}], \dots, \sqrt{\rho} \text{Im}[P_{v,K}], 0, 1]^T \quad (78)$$

with $\boldsymbol{\zeta} \sim \mathcal{N}(\mathbf{0}_{(2K+2)}, \frac{1}{2} \mathbf{I}_{(2K+2)})$, into (10), which gives

$$\begin{aligned} &\mathbb{E} \left[\text{sgn} \left(\sqrt{\rho} \sum_{i=1}^K (\text{Re}[H_{m,i}] \text{Re}[P_{u,i}] + \text{Im}[H_{m,i}] \text{Im}[P_{u,i}]) + \text{Re}[Z_{m,u}] \right) \right. \\ &\quad \left. \times \text{sgn} \left(\sqrt{\rho} \sum_{i=1}^K (\text{Re}[H_{m,i}] \text{Re}[P_{v,i}] + \text{Im}[H_{m,i}] \text{Im}[P_{v,i}]) + \text{Re}[Z_{m,v}] \right) \right] \\ &= \Omega \left(\frac{\rho \sum_{k=1}^K (\text{Re}[P_{u,k}] \text{Re}[P_{v,k}] + \text{Im}[P_{u,k}] \text{Im}[P_{v,k}])}{(\rho \sum_{k=1}^K (\text{Re}[P_{u,k}]^2 + \text{Im}[P_{u,k}]^2) + 1)^{\frac{1}{2}} (\rho \sum_{k=1}^K (\text{Re}[P_{v,k}]^2 + \text{Im}[P_{v,k}]^2) + 1)^{\frac{1}{2}}} \right). \end{aligned} \quad (79)$$

- Considering the third expectation term in (63), we have

$$\text{Re}[\text{tr}(\hat{\mathbf{H}}^H \mathbf{H})] = \sqrt{\frac{\rho K + 1}{2}} \Psi \text{Re} \left[\sum_{m=1}^M \sum_{k=1}^K \left(\sum_{u=1}^{\tau} P_{u,k} (A_{m,u} + j B_{m,u}) \right)^* H_{m,k} \right] \quad (80)$$

$$\begin{aligned} &= \sqrt{\frac{\rho K + 1}{2}} \Psi \sum_{m=1}^M \sum_{k=1}^K \sum_{u=1}^{\tau} (\text{Re}[P_{u,k}] \text{Re}[H_{m,k}] A_{m,u} + \text{Im}[P_{u,k}] \text{Im}[H_{m,k}] A_{m,u} \\ &\quad + \text{Re}[P_{u,k}] \text{Im}[H_{m,k}] B_{m,u} - \text{Im}[P_{u,k}] \text{Re}[H_{m,k}] B_{m,u}). \end{aligned} \quad (81)$$

Hence, the expected value of (81) is given by

$$\mathbb{E}[\text{Re}[\text{tr}(\hat{\mathbf{H}}^H \mathbf{H})]] = \sqrt{\frac{2}{\pi}} \rho \Psi M K \tau \quad (82)$$

where (82) follows from

$$\mathbb{E}[\text{Re}[H_{m,k}]A_{m,u}] = \mathbb{E}[\text{Im}[H_{m,k}]B_{m,u}] \quad (83)$$

$$= \frac{1}{\sqrt{\pi}} \sqrt{\frac{\rho}{\rho K + 1}} \text{Re}[p_u] \quad (84)$$

$$\mathbb{E}[\text{Im}[H_{m,k}]A_{m,u}] = -\mathbb{E}[\text{Re}[H_{m,k}]B_{m,u}] \quad (85)$$

$$= \frac{1}{\sqrt{\pi}} \sqrt{\frac{\rho}{\rho K + 1}} \text{Im}[p_u]. \quad (86)$$

Finally, the expression in (14) is obtained by plugging (72) and (82) into (63). ■

APPENDIX IV

PROOF OF PROPOSITION 2

Recalling the definitions in (64)–(67), we can write the $((u-1)M+m, (v-1)M+n)$ th entry of $\mathbf{r}_p \mathbf{r}_p^H$ as

$$R_{m,u} R_{n,v}^* = \frac{\rho K + 1}{2} (A_{m,u} + j B_{m,u}) (A_{n,v} + j B_{n,v})^* \quad (87)$$

$$= \frac{\rho K + 1}{2} (A_{m,u} A_{n,v} + B_{m,u} B_{n,v} + j (B_{m,u} A_{n,v} - A_{m,u} B_{n,v})) \quad (88)$$

with $R_{m,u} R_{m,u}^* = \rho K + 1$. Hence, from (73)–(75), we obtain

$$\mathbb{E}[R_{m,u} R_{n,v}^*] = \begin{cases} (\rho K + 1) \left(\Omega \left(\frac{\rho \sum_{k=1}^K \text{Re}[P_{u,k} P_{v,k}^*]}{\rho K + 1} \right) - j \Omega \left(\frac{\rho \sum_{k=1}^K \text{Im}[P_{u,k} P_{v,k}^*]}{\rho K + 1} \right) \right) & \text{if } m = n, u \neq v, \\ 0 & \text{if } m \neq n \end{cases} \quad (89)$$

and the expression in (35) readily follows. ■

APPENDIX V

PROOF OF THEOREM 3

We begin by introducing the following definitions:⁴

$$a_{m,u} \triangleq \text{sgn}(\text{Re}[\sqrt{\rho} h_m p_u^* + Z_{m,u}]) \quad (90)$$

$$= \text{sgn} \left(\sqrt{\rho} (\text{Re}[h_m] \text{Re}[p_u] + \text{Im}[h_m] \text{Im}[p_u]) + \text{Re}[Z_{m,u}] \right), \quad (91)$$

$$b_{m,u} \triangleq \text{sgn}(\text{Im}[\sqrt{\rho} h_m p_u^* + Z_{m,u}]) \quad (92)$$

$$= \text{sgn} \left(\sqrt{\rho} (-\text{Re}[h_m] \text{Im}[p_u] + \text{Im}[h_m] \text{Re}[p_u]) + \text{Im}[Z_{m,u}] \right) \quad (93)$$

⁴Note that (90)–(93) are equivalent to (64)–(67) for $K = 1$.

and

$$c_m \triangleq \text{sgn}(\text{Re}[\sqrt{\rho}h_ms_\ell + z_m]) \quad (94)$$

$$= \text{sgn}\left(\sqrt{\rho}(\text{Re}[h_m]\text{Re}[s_\ell] - \text{Im}[h_m]\text{Im}[s_\ell]) + \text{Re}[z_m]\right), \quad (95)$$

$$d_m \triangleq \text{sgn}(\text{Im}[\sqrt{\rho}h_ms_\ell + z_m]) \quad (96)$$

$$= \text{sgn}\left(\sqrt{\rho}(\text{Re}[h_m]\text{Im}[s_\ell] + \text{Im}[h_m]\text{Re}[s_\ell]) + \text{Im}[z_m]\right). \quad (97)$$

From (38), we can write the estimated symbol as

$$\hat{s}_\ell = \frac{\rho+1}{2}\sqrt{\Psi'} \sum_{m=1}^M \sum_{u=1}^{\tau} p_u^*(a_{m,u} + j b_{m,u})^*(c_m + j d_m) \quad (98)$$

$$= \frac{\rho+1}{2}\sqrt{\Psi'} \sum_{m=1}^M \sum_{u=1}^{\tau} p_u^*(a_{m,u}c_m + b_{m,u}d_m + j(a_{m,u}d_m - b_{m,u}c_m)). \quad (99)$$

Hence, the expression in (39) follows from

$$\mathbb{E}[a_{m,u}c_m] = \mathbb{E}[b_{m,u}d_m] \quad (100)$$

$$= \Omega\left(\frac{\rho\text{Re}[p_us_\ell]}{\sqrt{(\rho+1)(\rho|s_\ell|^2+1)}}\right), \quad (101)$$

$$\mathbb{E}[a_{m,u}d_m] = -\mathbb{E}[b_{m,u}c_m] \quad (102)$$

$$= \Omega\left(\frac{\rho\text{Im}[p_us_\ell]}{\sqrt{(\rho+1)(\rho|s_\ell|^2+1)}}\right) \quad (103)$$

which are derived again by applying Proposition 1. For instance, $\mathbb{E}[a_{m,u}c_m]$ in (100)–(101) can be obtained by plugging $\boldsymbol{\zeta} = [\text{Re}[h_m], \text{Im}[h_m], \text{Re}[Z_{m,u}], \text{Re}[z_m]]^T \sim \mathcal{N}(\mathbf{0}_4, \frac{1}{2}\mathbf{I}_4)$, $\mathbf{a}_1 = [\sqrt{\rho}\text{Re}[p_u], \sqrt{\rho}\text{Im}[p_u], 1, 0]^T$, and $\mathbf{a}_2 = [\sqrt{\rho}\text{Re}[s_\ell], -\sqrt{\rho}\text{Im}[s_\ell], 0, 1]^T$ into (10), which gives

$$\begin{aligned} & \mathbb{E}\left[\text{sgn}\left(\sqrt{\rho}(\text{Re}[h_m]\text{Re}[p_u] + \text{Im}[h_m]\text{Im}[p_u]) + \text{Re}[Z_{m,u}]\right)\right. \\ & \quad \times \left.\text{sgn}\left(\sqrt{\rho}(\text{Re}[h_m]\text{Re}[s_\ell] - \text{Im}[h_m]\text{Im}[s_\ell]) + \text{Re}[z_m]\right)\right] \\ & = \Omega\left(\frac{\rho(\text{Re}[p_u]\text{Re}[s_\ell] - \text{Im}[p_u]\text{Im}[s_\ell])}{\sqrt{\rho(\text{Re}[p_u]^2 + \text{Im}[p_u]^2) + 1}\sqrt{\rho(\text{Re}[s_\ell]^2 + \text{Im}[s_\ell]^2) + 1}}\right). \end{aligned} \quad (104)$$

■

APPENDIX VI

PROOF OF THEOREM 4

The variance of the estimated symbol \hat{s}_ℓ can be written as

$$\mathbf{V}_\ell = \mathbb{E}[|\hat{s}_\ell|^2] - |\mathbf{E}_\ell|^2 \quad (105)$$

where $\mathbb{E}[|\hat{s}_\ell|^2] = \mathbb{E}[\text{Re}[\hat{s}_\ell]^2] + \mathbb{E}[\text{Im}[\hat{s}_\ell]^2]$ and (cf. (39))

$$\begin{aligned}
|E_\ell|^2 = & (\rho+1)^2 \Psi' M^2 \sum_{u=1}^{\tau} \sum_{v=1}^{\tau} \left(\text{Re}[p_u^* p_v] \left(\Omega \left(\frac{\rho \text{Re}[p_u s_\ell]}{\sqrt{(\rho+1)(\rho|s_\ell|^2+1)}} \right) \Omega \left(\frac{\rho \text{Re}[p_v s_\ell]}{\sqrt{(\rho+1)(\rho|s_\ell|^2+1)}} \right) \right. \right. \\
& + \Omega \left(\frac{\rho \text{Im}[p_u s_\ell]}{\sqrt{(\rho+1)(\rho|s_\ell|^2+1)}} \right) \Omega \left(\frac{\rho \text{Im}[p_v s_\ell]}{\sqrt{(\rho+1)(\rho|s_\ell|^2+1)}} \right) \Big) \\
& + \text{Im}[p_u^* p_v] \left(\Omega \left(\frac{\rho \text{Re}[p_u s_\ell]}{\sqrt{(\rho+1)(\rho|s_\ell|^2+1)}} \right) \Omega \left(\frac{\rho \text{Im}[p_v s_\ell]}{\sqrt{(\rho+1)(\rho|s_\ell|^2+1)}} \right) \right. \\
& \left. \left. - \Omega \left(\frac{\rho \text{Im}[p_u s_\ell]}{\sqrt{(\rho+1)(\rho|s_\ell|^2+1)}} \right) \Omega \left(\frac{\rho \text{Re}[p_v s_\ell]}{\sqrt{(\rho+1)(\rho|s_\ell|^2+1)}} \right) \right) \right). \tag{106}
\end{aligned}$$

Furthermore, recalling the definitions in (90)–(97) and building on (98)–(99), we obtain

$$\begin{aligned}
\text{Re}[\hat{s}_\ell]^2 = & \frac{(\rho+1)^2}{4} \Psi' \left(\sum_{m=1}^M \sum_{u=1}^{\tau} (\text{Re}[p_u](a_{m,u}c_m + b_{m,u}d_m) + \text{Im}[p_u](a_{m,u}d_m - b_{m,u}c_m)) \right)^2 \tag{107} \\
= & \frac{(\rho+1)^2}{4} \Psi' \left(\sum_{m=1}^M \sum_{u=1}^{\tau} (\text{Re}[p_u](a_{m,u}c_m + b_{m,u}d_m) + \text{Im}[p_u](a_{m,u}d_m - b_{m,u}c_m)) \right. \\
& + \sum_{m=1}^M \sum_{u \neq v} (\text{Re}[p_u](a_{m,u}c_m + b_{m,u}d_m) + \text{Im}[p_u](a_{m,u}d_m - b_{m,u}c_m)) \\
& \times (\text{Re}[p_v](a_{m,v}c_m + b_{m,v}d_m) + \text{Im}[p_v](a_{m,v}d_m - b_{m,v}c_m)) \\
& + \sum_{m \neq n} \sum_{u=1}^{\tau} \sum_{v=1}^{\tau} (\text{Re}[p_u](a_{m,u}c_m + b_{m,u}d_m) + \text{Im}[p_u](a_{m,u}d_m - b_{m,u}c_m)) \\
& \left. \times (\text{Re}[p_v](a_{n,v}c_n + b_{n,v}d_n) + \text{Im}[p_v](a_{n,v}d_n - b_{n,v}c_n)) \right) \tag{108}
\end{aligned}$$

and $\text{Im}[\hat{s}_\ell]^2$ can be obtained following similar steps. Then, summing up (108) and $\text{Im}[\hat{s}_\ell]^2$ yields

$$\begin{aligned}
|\hat{s}_\ell|^2 = & \frac{(\rho+1)^2}{4} \Psi' \left(4M\tau + 2 \sum_{m=1}^M \sum_{u \neq v} (\text{Re}[p_u^* p_v](a_{m,u}a_{m,v} + b_{m,u}b_{m,v}) \right. \\
& - \text{Im}[p_u^* p_v](a_{m,u}b_{m,v} - b_{m,u}a_{m,v})) \\
& + \sum_{m \neq n} \sum_{u=1}^{\tau} \sum_{v=1}^{\tau} \left(\text{Re}[p_u^* p_v]((a_{m,u}c_m + b_{m,u}d_m)(a_{n,v}c_n + b_{n,v}d_n) \right. \\
& + (a_{m,u}d_m - b_{m,u}c_m)(a_{n,v}d_n - b_{n,v}c_n)) \\
& + \text{Im}[p_u^* p_v]((a_{m,u}c_m + b_{m,u}d_m)(a_{n,v}d_n - b_{n,v}c_n) \\
& \left. \left. - (a_{m,u}d_m - b_{m,u}c_m)(a_{n,v}c_n + b_{n,v}d_n)) \right) \right). \tag{109}
\end{aligned}$$

Now, we have that $\xi_{m,u} \in \{a_{m,u}, b_{m,u}, c_m, d_m\}$ and $\xi_{n,v} \in \{a_{n,v}, b_{n,v}, c_n, d_n\}$ are independent random variables if $m \neq n$ regardless of the indices u, v . This implies that $\mathbb{E}[a_{m,u}c_m b_{n,v}d_n] = \mathbb{E}[a_{m,u}c_m]\mathbb{E}[b_{n,v}d_n]$ and the same holds for the other products in the second summation of (109).

Hence, the expected value of (109) is given by

$$\begin{aligned}
\mathbb{E}[|\hat{s}_\ell|^2] &= (\rho + 1)^2 \Psi' M \left(\tau + \sum_{u \neq v} \left(\text{Re}[p_u^* p_v] \Omega \left(\frac{\rho \text{Re}[p_u p_v^*]}{\rho + 1} \right) - \text{Im}[p_u^* p_v] \Omega \left(\frac{\rho \text{Im}[p_u p_v^*]}{\rho + 1} \right) \right) \right. \\
&\quad + (M - 1) \sum_{u=1}^{\tau} \sum_{v=1}^{\tau} \text{Re}[p_u^* p_v] \left(\Omega \left(\frac{\rho \text{Re}[p_u s_\ell]}{\sqrt{(\rho + 1)(\rho |s_\ell|^2 + 1)}} \right) \Omega \left(\frac{\rho \text{Re}[p_v s_\ell]}{\sqrt{(\rho + 1)(\rho |s_\ell|^2 + 1)}} \right) \right. \\
&\quad \left. \left. + \Omega \left(\frac{\rho \text{Im}[p_u s_\ell]}{\sqrt{(\rho + 1)(\rho |s_\ell|^2 + 1)}} \right) \Omega \left(\frac{\rho \text{Im}[p_v s_\ell]}{\sqrt{(\rho + 1)(\rho |s_\ell|^2 + 1)}} \right) \right) \right. \\
&\quad + (M - 1) \sum_{u=1}^{\tau} \sum_{v=1}^{\tau} \text{Im}[p_u^* p_v] \left(\Omega \left(\frac{\rho \text{Re}[p_u s_\ell]}{\sqrt{(\rho + 1)(\rho |s_\ell|^2 + 1)}} \right) \Omega \left(\frac{\rho \text{Im}[p_v s_\ell]}{\sqrt{(\rho + 1)(\rho |s_\ell|^2 + 1)}} \right) \right. \\
&\quad \left. \left. - \Omega \left(\frac{\rho \text{Im}[p_u s_\ell]}{\sqrt{(\rho + 1)(\rho |s_\ell|^2 + 1)}} \right) \Omega \left(\frac{\rho \text{Re}[p_v s_\ell]}{\sqrt{(\rho + 1)(\rho |s_\ell|^2 + 1)}} \right) \right) \right) \quad (110)
\end{aligned}$$

where (110) follows from (100)–(103) and from⁵

$$\mathbb{E}[a_{m,u} a_{m,v}] = \mathbb{E}[b_{m,u} b_{m,v}] \quad (111)$$

$$= \Omega \left(\frac{\rho \text{Re}[p_u p_v^*]}{\rho + 1} \right), \quad (112)$$

$$\mathbb{E}[a_{m,u} b_{m,v}] = \Omega \left(\frac{\rho \text{Im}[p_u p_v^*]}{\rho + 1} \right). \quad (113)$$

Finally, the expression in (41) is obtained by plugging (106) and (110) into (105). \blacksquare

REFERENCES

- [1] N. Rajatheva, I. Atzeni, E. Björnson *et al.*, “White paper on broadband connectivity in 6G,” June 2020. [Online]. Available: <http://jultika.oulu.fi/files/isbn9789526226798.pdf>
- [2] F. Rusek, D. Persson, B. K. Lau, E. G. Larsson, T. L. Marzetta, O. Edfors, and F. Tufvesson, “Scaling up MIMO: Opportunities and challenges with very large arrays,” *IEEE Signal Process. Mag.*, vol. 30, no. 1, pp. 40–60, Jan. 2013.
- [3] M. Xiao, S. Mumtaz, Y. Huang *et al.*, “Millimeter wave communications for future mobile networks,” *IEEE J. Sel. Areas Commun.*, vol. 35, no. 9, pp. 1909–1935, Sept. 2017.
- [4] J. Mo and R. W. Heath, “Capacity analysis of one-bit quantized MIMO systems with transmitter channel state information,” *IEEE Trans. Signal Process.*, vol. 63, no. 20, pp. 5498–5512, Oct. 2015.
- [5] C. Studer and G. Durisi, “Quantized massive MU-MIMO-OFDM uplink,” *IEEE Trans. Commun.*, vol. 64, no. 6, pp. 2387–2399, June 2016.
- [6] J. Choi, J. Mo, and R. W. Heath, “Near maximum-likelihood detector and channel estimator for uplink multiuser massive MIMO systems with one-bit ADCs,” *IEEE Trans. Commun.*, vol. 64, no. 5, pp. 2005–2018, May 2016.
- [7] Y. Li, C. Tao, G. Seco-Granados, A. Mezghani, A. L. Swindlehurst, and L. Liu, “Channel estimation and performance analysis of one-bit massive MIMO systems,” *IEEE Trans. Signal Process.*, vol. 65, no. 15, pp. 4075–4089, Aug. 2017.
- [8] A. K. Saxena, I. Fijalkow, and A. L. Swindlehurst, “Analysis of one-bit quantized precoding for the multiuser massive MIMO downlink,” *IEEE Trans. Signal Process.*, vol. 65, no. 17, pp. 4624–4634, Sept. 2017.

⁵Note that (111)–(113) are equivalent to (73)–(75) for $K = 1$.

- [9] S. Jacobsson, G. Durisi, M. Coldrey, U. Gustavsson, and C. Studer, "Throughput analysis of massive MIMO uplink with low-resolution ADCs," *IEEE Trans. Wireless Commun.*, vol. 16, no. 6, pp. 1304–1309, Jun. 2017.
- [10] S. Jacobsson, G. Durisi, M. Coldrey, T. Goldstein, and C. Studer, "Quantized precoding for massive MU-MIMO," *IEEE Trans. Commun.*, vol. 65, no. 11, pp. 4670–4684, Nov. 2017.
- [11] S. Jacobsson, G. Durisi, M. Coldrey, and C. Studer, "Linear precoding with low-resolution DACs for massive MU-MIMO-OFDM downlink," *IEEE Trans. Wireless Commun.*, vol. 18, no. 3, pp. 1595–1609, Mar. 2019.
- [12] J. Singh, O. Dabeer, and U. Madhow, "On the limits of communication with low-precision analog-to-digital conversion at the receiver," *IEEE Trans. Commun.*, vol. 57, no. 12, pp. 3629–3639, Dec. 2009.
- [13] N. Liang and W. Zhang, "Mixed-ADC massive MIMO," *IEEE J. Sel. Areas Commun.*, vol. 34, no. 4, pp. 983–997, Apr. 2016.
- [14] C. Mollén, J. Choi, E. G. Larsson, and R. W. Heath, "Uplink performance of wideband massive MIMO with one-bit ADCs," *IEEE Trans. Wireless Commun.*, vol. 16, no. 1, pp. 87–100, Jan. 2017.
- [15] S. Wang, Y. Li, and J. Wang, "Multiuser detection in massive spatial modulation MIMO with low-resolution ADCs," *IEEE Trans. Wireless Commun.*, vol. 14, no. 4, pp. 2156–2168, Sept. 2015.
- [16] Y.-S. Jeon, N. Lee, S. Hong, and R. W. Heath, "One-bit sphere decoding for uplink massive MIMO systems with one-bit ADCs," *IEEE Trans. Wireless Commun.*, vol. 17, no. 7, pp. 4509–4521, July 2018.
- [17] C.-K. Wen, C.-J. Wang, S. Jin, K.-K. Wong, and P. Ting, "Bayes-optimal joint channel-and-data estimation for massive MIMO with low-precision ADCs," *IEEE Trans. Signal Process.*, vol. 64, no. 10, pp. 2541–2556, May 2016.
- [18] J. J. Bussgang, "Crosscorrelation functions of amplitude-distorted Gaussian signals," Res. Lab. Electron., Massachusetts Inst. Technol., Tech. Rep., 1952.
- [19] Y. Li, C. Tao, A. Lee Swindlehurst, A. Mezghani, and L. Liu, "Downlink achievable rate analysis in massive MIMO systems with one-bit DACs," *IEEE Commun. Lett.*, vol. 21, no. 7, pp. 1669–1672, July 2017.
- [20] M. S. Stein, S. Bar, J. A. Nossek, and J. Tabrikian, "Performance analysis for channel estimation with 1-bit ADC and unknown quantization threshold," *IEEE Trans. Signal Process.*, vol. 66, no. 10, pp. 2557–2571, May 2018.
- [21] J. Mo, P. Schniter, and R. W. Heath, "Channel estimation in broadband millimeter wave MIMO systems with few-bit ADCs," *IEEE Trans. Signal Process.*, vol. 66, no. 5, pp. 1141–1154, Mar. 2018.
- [22] S. Rao, A. Mezghani, and A. L. Swindlehurst, "Channel estimation in one-bit massive MIMO systems: Angular versus unstructured models," *IEEE J. Sel. Topics Signal Process.*, vol. 13, no. 5, pp. 1017–1031, Sept. 2019.
- [23] Y.-S. Jeon, N. Lee, and H. V. Poor, "Robust data detection for MIMO systems with one-bit ADCs: A reinforcement learning approach," *IEEE Trans. Wireless Commun.*, vol. 19, no. 3, pp. 1663–1676, Mar. 2020.
- [24] L. V. Nguyen, D. T. Ngo, N. H. Tran, A. L. Swindlehurst, and D. H. N. Nguyen, "Supervised and semi-supervised learning for MIMO blind detection with low-resolution ADCs," *IEEE Trans. Wireless Commun.*, vol. 19, no. 4, pp. 2427–2442, Apr. 2020.
- [25] M. Shao, Q. Li, W.-K. Ma, and A. M.-C. So, "A framework for one-bit and constant-envelope precoding over multiuser massive MISO channels," *IEEE Trans. Signal Process.*, vol. 67, no. 20, pp. 5309–5324, Oct. 2019.
- [26] M. Hyder and K. Mahata, "Zadoff-Chu sequence design for random access initial uplink synchronization in LTE-like systems," *IEEE Trans. Wireless Commun.*, vol. 16, no. 1, pp. 503–511, Jan. 2017.
- [27] I. G. Abrahamson, "Orthant probabilities for the quadrivariate normal distribution," *The Ann. Math. Statist.*, vol. 35, no. 4, pp. 1685–1703, Dec. 1964.